PSEUDOCLASSICAL TRANSPORT IN A SHEARED MAGNETIC FIELD:
- THEORY AND SIMULATION -

Memorandum No. UCB/ERL M77/76

16 December 1977

ELECTRONICS RESEARCH LABORATORY
College of Engineering
UNIVERSITY OF CALIFORNIA, BERKELEY
94720

TABLE OF CONTENTS i

ABSTRACT

The cross field transport due to the trapping of electrons in a finite amplitude wave (pseudoclassical transport) is investigated. Both finite wave frequencies and magnetic shear are included. The single particle orbit equations are solved to obtain the trapping criterion as well as the trapped particle orbit width and bounce frequency. Using a random walk model, the scaling of the pseudoclassical transport coefficients with the parameters of the plasma and wave are deduced. This scaling is employed to extend a previous calculation of the transport coefficients to include magnetic shear. Magnetic shear is found to reduce these transport coefficients. Computer simulations of this transport process are presented. The measured transport rates are in very good agreement with the previous kinetic calculation in the absence of magnetic shear, and with this extension of pseudoclassical transport theory which includes magnetic shear.

I. INTRODUCTION

Low frequency waves, which are universally present in inhomogeneous plasmas, are thought to be responsible for the anomalous transport observed in tokamaks (Dean, et al., 1974). In this paper we investigate the transport associated with a coherent electrostatic wave propagating in a nearly collisionless, magnetized plasma. In previous work, the transport coefficients associated with the trapping of electrons by a finite amplitude drift wave in a uniform magnetic field have been calculated (Pogutse, 1972; Gell and Nevins, 1975; Nevins, 1977a). Other workers have considered the effect of shear, but in a time independent electric field (Brimbilla and Lichtenberg, 1973). Here, this work is extended to include both finite wave frequencies and shear in the magnetic field. Preliminary results were reported earlier (Gell, et al., 1975). Magnetic shear is found to reduce the transport coefficients, and hence, to reduce the nonlinear growth rate of the finite amplitude wave (Nevins, 1977b; Nevins, 1977c).

Investigation of the anomalous transport associated with a single wave is useful as a basis for understanding the anomalous transport associated with a spectrum of waves. It is particularly relevant to systems in which the wave spectrum is sharply peaked. Such coherent drift wave spectra have recently been observed in toroidal plasmas with strong magnetic shear (Okabayashi and Arunasalem, 1977; Vojtsenya, et al., 1977), while recent work (Koch and Tang, 1977) suggests that the drift wave spectrum observed in tokamak plasmas (Mazzucato, 1976; Surko and Slusher, 1976) is more coherent than previously reported.

We consider waves with phase velocities, $v_\phi = \omega/k_\parallel$, in the range

$$v_{ti} \ll v_\phi \ll v_{te} \tag{1.1}$$

where $v_{ti} = (T_i/m_i)^{\frac{1}{2}}$ and $v_{te} = (T_e/m_e)^{\frac{1}{2}}$ are the electron and ion thermal velocities, $k_\parallel$ is the component of the wave vector parallel to the magnetic field, and ω is the wave frequency. Low frequency drift waves satisfying inequality (1.1) have been both predicted theoretically (see, e.g., Galeev, et al., 1963; Kadomtsev and Pogutse, 1969), and observed experimentally in Q-machines (see, e.g., Politzer, 1971; Prager, et al., 1974) and tokamaks (e.g., Mazzucato, 1976; Surko and Slusher, 1976). In addition, we restrict our attention to the electron transport rates, as the anomalous losses observed in tokamaks are attributed to an enhancement of the electron transport coefficients over the neoclassical values (Dean, et al., 1974).

A mechanism for the transport of particles and/or energy across the magnetic field requires motion of the particles relative to the magnetic lines of force and a finite correlation time. From this viewpoint, classical transport (Rosenbluth and Kaufman, 1958) results from the gyration of particles about the magnetic field lines combined with a correlation time determined by binary collisions.

In neoclassical transport theory the gyration of particles about the magnetic field lines is ignored. The particle motion relative to the magnetic field lines is provided, instead, by the drifts of the particle guiding centers in the inhomogeneous magnetic field (see, e.g., Galeev and Sagdeev, 1968; Rosenbluth, et. al., 1972; Hazeltine and Hinton, 1976), while the correlation time is still determined by binary collisions.

This paper considers pseudoclassical transport. The name "pseudoclassical" has been adopted by several authors (Pogutse, 1972; Yoshikawa and Christofolis, 1972; Gell, et. al., 1975) to describe a sequence of related transported mechanisms in which the particle motion relative to the magnetic field is provided by the guiding center drifts in the electric field of a low frequency electrostatic wave rather than the ∇B drifts of neoclassical theory. The correlation time is again determined by binary collisions.

Pseudoclassical transport theory bears a close analogy to neoclassical transport theory in that

1) it is only necessary to follow the motion of particle guiding centers,
2) between collisions particles are subject to guiding center drifts that vary periodically in time, and
3) at sufficiently low collision frequencies particle trapping occurs.

We find that, like neoclassical theory, pseudoclassical transport theory has three collision frequency regimes: a low collision frequency regime in which the transport coefficients are proportional to the collision frequency, an intermediate collision frequency regime in which the transport is properly described by the "quasilinear" transport coefficients (see, e.g., Horton, 1976), and, hence, is independent of the collision frequency, and finally a high collision frequency regime investigated by Yoshikawa and Christofolis (1971).

In both neoclassical and pseudoclassical transport theory the collision frequency regime is determined by the dimensionless parameter

$$\nu_* = \frac{90^\circ \text{ collision frequency}}{\text{transit frequency}} \quad . \tag{1.2}$$

In pseudoclassical theory ν_* is given by

$$\nu_* = \frac{\nu_e}{k_\parallel v_{te}} \tag{1.3}$$

where, following Braginskii (1965), we take

$$\nu_e = \frac{4(2\pi)^{\frac{1}{2}} e^4}{3m^{\frac{1}{2}} T^{3/2}} \ell n \, \Lambda \quad . \tag{1.4}$$

When ν_* is small, the transport is dominated by resonant particles which ExB drift across the magnetic field in a slowly varying electric field.

To emphasize the analogy between pseudoclassical transport and neoclassical transport we shall refer to the low collision frequency regime of pseudoclassical transport as the "pineapple" regime, and the orbits of particles trapped by the electrostatic wave will be referred to as "pineapple orbits". The reader may notice a resemblance between the trapped particle orbit shown in Fig. 2 and a pineapple.

This paper is primarily concerned with the "pineapple" regime of pseudoclassical transport theory in which the transport is dominated by those electrons which have become trapped in the electric field of the

low frequency wave. This regime of pseudoclassical transport was originally investigated by Pogutse (1972). The calculation of the pseudoclassical transport coefficients from kinetic theory was refined by later authors (Gell and Nevins, 1975; Nevins, 1977a). The effect of magnetic shear on the orbits of the electrostatically trapped particles was ignored in these calculations.

The pseudoclassical transport coefficients obtained by these authors depend upon $k_{\|}$. In a sheared magnetic field $k_{\|}$ is a function of x . When this spatial dependence is included, the pseudoclassical transport coefficients diverge at the mode rational surface, where $k_{\|}$ vanishes.

Brambilla and Lichtenberg (1973) have shown that this divergence is avoided when the effect of magnetic shear on the trapped particle orbits is considered. However, the formalism of Brambilla and Lichtenberg describes only the orbits of particles trapped near the mode rational surface in a time independent potential. Hence, it is not clear how the pineapple orbits of Brambilla and Lichtenberg are related to those of Pogutse.

In this paper we present a unified treatment of the pineapple orbits that allows both magnetic shear and a finite wave frequency. Our expression for the pineapple orbit width reduces to that obtained by Pogutse or Brambilla and Lichtenberg in the appropriate limit. This analysis of the pineapple orbits has been reported previously, together with some preliminary estimates of the pseudoclassical transport coefficients (Gell et al., 1975). The analysis is extended here with more detailed calculations of the transport coefficients.

In Section 2 we describe our model and introduce two constants of the particle motion.

In Section 3 an equation which describes the orbits of particles moving under the influence of both a sheared magnetic field and a low frequency electrostatic wave is derived.

In Section 4, restricting our attention to particle orbits that do not cross the mode rational surface (where $k_{\|}$ vanishes), we obtain expressions for both the pineapple orbit width, the fraction of particles that will be trapped in a given wave, and the bounce frequency of these electrostatically trapped particles. These quantities are necessary to predict the scaling of the pseudoclassical transport coefficients with the parameters of the system.

In Section 5 a random walk model is employed to determine the scaling of the pseudoclassical transport coefficients with the plasma parameters ν_e , B , and L_s ; as well as the wave parameters ω , $\underline{k}$, and ($e\phi_o/T$). These scaling laws allow us to generalize the expressions for the pseudoclassical transport coefficients, obtained previously from kinetic theory (Nevins, 1977) in the limit of vanishing magnetic shear, to the case of a sheared magnetic field.

In Section 6 the results of computer simulations (using non-interacting particles) of pseudoclassical transport are presented. The values of the pseudoclassical diffusion coefficient as measured in the simulations are found to be in very good agreement with the theoretical values of Section 5.

Finally, in Section 7 we conclude by examining the spatial dependence of the pseudoclassical transport coefficients and estimating the pseudoclassical energy containment time.

2. THE GUIDING CENTER EQUATIONS AND SOME CONSTANTS OF THE MOTION

The model used to study pseudoclassical transport is a slab in which the magnetic field lies in the y-z plane. Magnetic shear in included by allowing the direction of the magnetic field to vary with x. The scale length for variations in the direction of the magnetic field is L_s (see Fig. 1). A finite amplitude traveling wave is propagating in the y-z plane. This wave is assumed to be electrostatic. It may be described by the potential

$$\Phi = \Phi_o h(\theta) \tag{2.1}$$

where the wave phase, θ, is given by

$$\theta = \underline{k}\cdot\underline{r} - \omega t . \tag{2.2}$$

Φ_o is the wave amplitude, while $h(\theta)$ is a function that describes the wave form. This function is assumed to have a maximum value of one.

The coordinate system is chosen such that

$$\underline{k} = k\hat{y} \tag{2.3}$$

and our analysis is restricted to the case in which

$$k\rho_e,\ \rho_e/L_s,\ \omega/\Omega_e \ll 1 \tag{2.4}$$

where $\Omega_e=(eB/m)$ is the electron gyrofrequency, and $\rho_e = (v_{te}/\Omega_e)$ is the electron gyroradius. In this limit the particle motion is well approsimated by the motion of its guiding center.

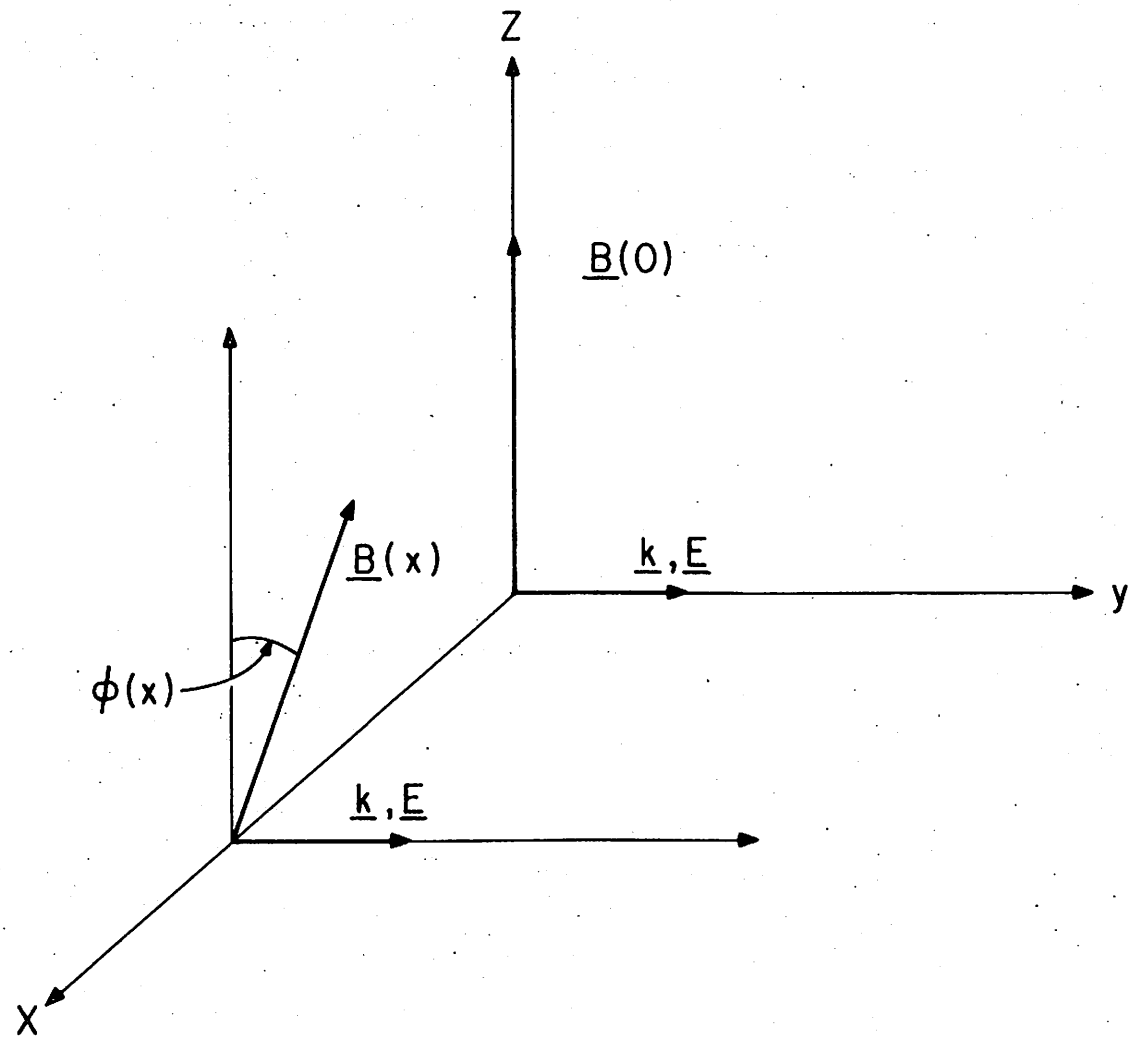

FIGURE 1. The Configuration of our Model.

Using the variable set $(x, \theta, v_\parallel)$, where $v_\parallel$ is the component of the particle's velocity parallel to the magnetic field, the guiding center equations of motion are

$$\frac{dx}{dt} = - \frac{k_\perp}{B} \Phi_o \, h'(\theta) \tag{2.5}$$

$$\frac{d\theta}{dt} = k_\parallel v_\parallel - \omega \tag{2.6}$$

$$\frac{dv_\parallel}{dt} = - k_\parallel \frac{e}{m} \Phi_o \, h'(\theta) \tag{2.7}$$

where

$$h'(\theta) = \frac{dh}{d\theta} \tag{2.8}$$

and

$$k_\perp(x) = \frac{B_z(x)}{B} k \tag{2.9}$$

$$k_\parallel(x) = \frac{B_y(x)}{B} k \, . \tag{2.10}$$

These guiding center equations of motion are accurate through zero order in ρ_e/L_s. This level of approximation is sufficient for our purposes, as we are interested in effects of order $(\Delta x_p/L_s)$; where Δx_p, the pineapple orbit width, is assumed to be large compared to ρ_e. Figure 2 illustrates the approximation made here by comparing the orbit

of a trapped particle as described by these guiding center equations with the orbit obtained by numerically integrating the equations of motion using the full Lorentz force.

Particles may be labeled by their phase coordinates at a particular time, $t = t_o$:

$$\begin{aligned} x_o &= x\,(t=t_o) \\ \theta_o &= \theta\,(t=t_o) \\ v_{\|o} &= v_\|(t=t_o)\ . \end{aligned} \tag{2.11}$$

At some later time t the particle phase coordinates may be expressed in terms of the change from their values at t_o ,

$$\begin{aligned} \delta x(t) &= x\,(t) - x_o \\ \delta\theta(t) &= \theta(t) - \theta_o \\ \delta v_\|(t) &= v_\|(t) - v_{\|o}\ . \end{aligned} \tag{2.12}$$

The change in wave potential at the particle is given by

$$\delta\Phi(t) = \Phi[\theta(t)] - \Phi(\theta_o)\ . \tag{2.13}$$

The guiding center equations of motion contain much more information than is required. These equations can be reduced to a system of two orbit equations by combining Eqs. (2.5) and (2.7) to obtain

$$dv_\| = \frac{e}{m} B \frac{k_\|}{k_\perp} dx \tag{2.14}$$

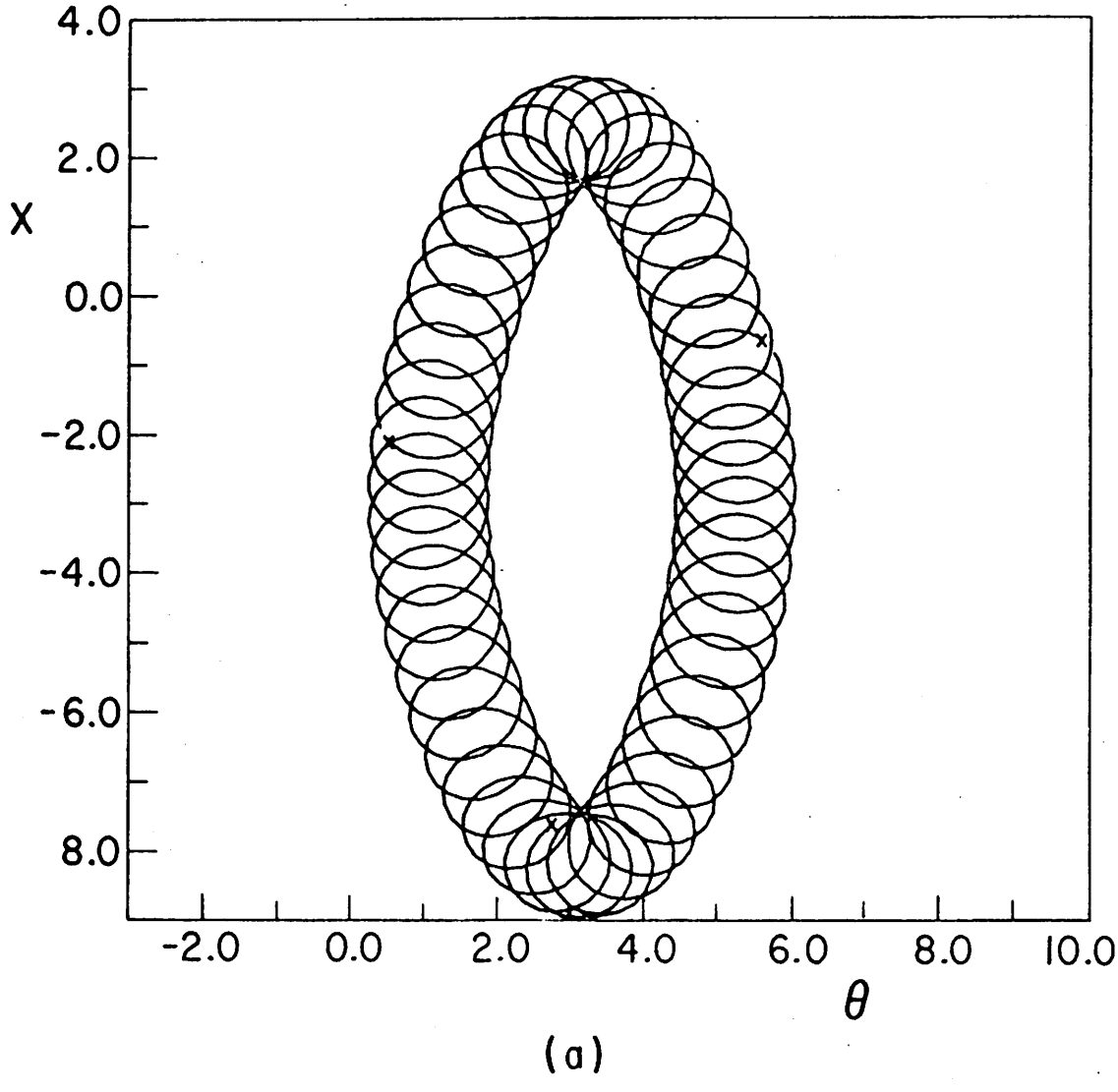

FIGURE 2. Projection of a trapped particle orbit into the x-θ plane ($k\rho_e$ and ω_{BOUNCE}/ω were chosen as 0.28 and 1/30 so that the particle's gyromotion could be clearly seen in (a)):

(a) integrating the equations of motion using the Lorentz force;

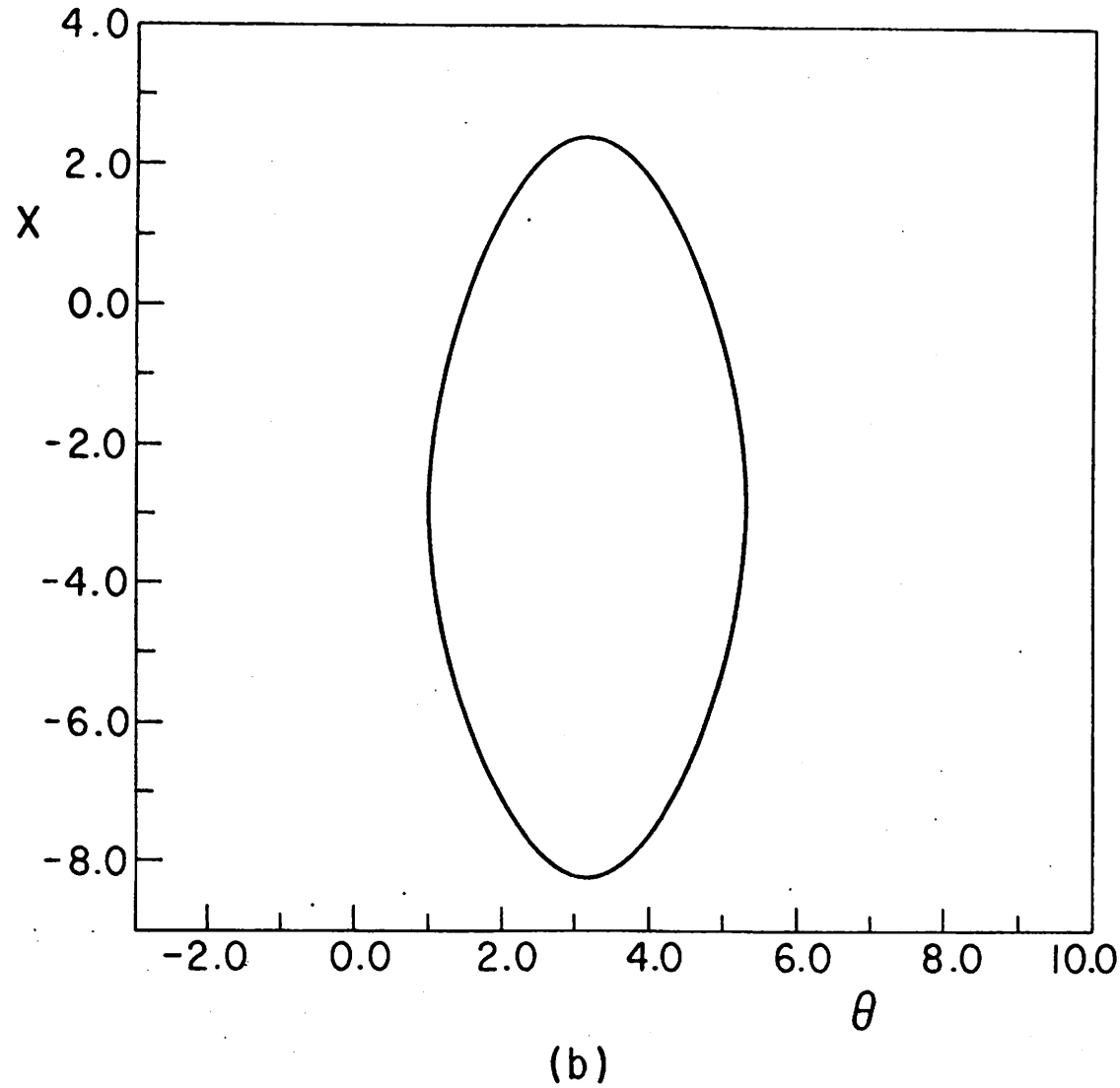

FIGURE 2 (cont.):

(b) the motion of the guiding center.

while Eqs. (2.5) and (2.6) may be combined to yield

$$(k_{\|} v_{\|} - \omega)\, dx = - \frac{k_{\perp}}{B}\, d\Phi \,. \tag{2.15}$$

Equations (2.14) and (2.15) will be integrated in Section 3 to obtain relations between δx, $\delta v_{\|}$, and $\delta \Phi$. Neither the wave phase θ nor the time t enter these relations. This reduction in the number of variables is possible due to the existence of two constants of the particle motion, namely a canonical momentum,

$$P_z = m v_z - e \int^x B_y(x')\, dx' \,, \tag{2.16}$$

and an energy constant,

$$E = \tfrac{1}{2} m \left(v_{\|} - \frac{\omega}{k} \frac{B_y}{B} \right)^2 + e\Phi - e \frac{\omega}{k} \int^x B_z(x')\, dx' + \mu B \tag{2.17}$$

where μ is the magnetic moment. This energy constant is discussed further in Appendix A.

The equivalence between these constants of the motion and the two differential relations, Eqs. (2.14) and (2.15) may be demonstrated by taking the total differential of Eqs. (2.16) and (2.17). In our model

$$v_z = v_{\|} \cos \phi \tag{2.18}$$

where $\phi(x)$ is the angle between the magnetic field vector and the z axis (see Fig. 1). Hence, dv_z may be expressed in terms of $dv_{\|}$ and dx as

$$dv_z = \cos\phi\, dv_\parallel - \sin\phi\, v_\parallel \frac{d\phi}{dx}\, dx \ . \qquad (2.19)$$

Taking the total differential of Eq. (2.16), and requiring that the z component of the momentum be conserved, we find

$$dp_z = 0 = m\cos\phi\, dv_\parallel - m\sin\phi\, v_\parallel \frac{d\phi}{dx}\, dx - e\, B_y\, dx \ , \qquad (2.20)$$

from which it follows that

$$dv_\parallel = \frac{e}{m} B \frac{k_\parallel}{k_\perp} \left(1 + \frac{v_\parallel}{\Omega} \frac{d\phi}{dx}\right) dx \ . \qquad (2.21)$$

The second term in parenthesis, $(v_\parallel/\Omega)(d\phi/dx)$, is of order ρ_e/L_s . In writing Eqs. (2.3) - (2.5) terms of this order were ignored. Hence, we may neglect this term in Eq. (2.21), recovering Eq. (2.14).

Similarly, we may take the total differential of Eq. (2.17), and demand that the energy constant E be conserved. Using Eq. (2.14), and ignoring terms in (ω/Ω) and (ρ_e/L) then yields

$$dE = 0 = \frac{eB}{k_\perp} (k_\parallel v_\parallel - \omega)\, dx + e\, d\Phi \qquad (2.22)$$

from which we immediately recover Eq. (2.15).

3. ORBIT EQUATIONS

In this Section an expression for the trapped particle orbit width that allows for traveling waves, finite values of $k_\parallel$ and shear in the magnetic field is devloped. The orbit widths obtained by Pogutse (1972), and by Brambilla and Lichtenberg (1973) are recovered by taking the appropriate limit of our more general expression.

The magnetic field configuration enters Eqs. (2.14) and (2.15) through the dependence of the coefficients $B(k_\parallel/k_\perp)$ and $k_\perp/B$ on x. The third x-dependent coefficient, $k_\parallel$, is simply the product of the first two. Waves with wave vectors nearly perpendicular to $\underline{B}$ are of greatest interest as they will yield pineapple orbit widths that are substantially greater than the gyroradius at modest values of the wave amplitude Φ_o. Inhomogeneous plasmas support several waves that meet these requirements. Perhaps the most important example is the low frequency drift wave (see, e.g., Kadomtsev, 1965; Mikhailovskii, 1974; Horton, 1976), which has been observed in many experimental plasmas (see, e.g., Politzer, 1971; Prager, et al., 1974; Mazzucato, 1976; Surko and Slusher, 1976; Okabayashi and Arunsasalem, 1977).

Without loss of generality, the coordinate system may be chosen such that $k_\parallel$ vanishes at $x=0$. A simple way of modeling shear in the magnetic field is to choose the x-dependence of the coefficients in Eqs. (2.14) and (2.15) to be

$$B(x)\,\frac{k_\parallel(x)}{k_\perp(x)} = B\frac{x}{L_s} \tag{3.1}$$

and

$$\frac{k_{\perp}(x)}{B(x)} = \frac{k}{B} , \tag{3.2}$$

from which it follows that

$$k_{\parallel}(x) = k\frac{x}{L_s} . \tag{3.3}$$

In these equations B is the magnitude of the magnetic field and L_s is the shear length. Equations (3.1) - (3.3) may be viewed as the leading terms in a power series expansion in (x/L_s) about $x = 0$. In general one could include higher order terms in this expansion. The leading terms, as given by Eqs. (3.1) - (3.3) are sufficient to understand the rather complicated particle orbits that are obtained by numerical integration of the guiding center equations of motion and to estimate the enhanced transport associated with these waves.

Combining Eqs. (2.14) and (3.1) we find, after one integration, that the change in the parallel velocity and the change in the guiding center position along particle orbits are related by

$$\frac{\delta v_{\parallel}}{u} = \frac{\delta x}{x_o} + \tfrac{1}{2}\left(\frac{\delta x}{x_o}\right)^2 \tag{3.4}$$

where

$$u \equiv \frac{e}{m} B \frac{x_o^2}{L_s} . \tag{3.5}$$

Equation (3.4) together with Eqs. (2.12) allows us to express the parallel velocity of a particle as a function of its guiding center position,

$$\frac{v_\parallel}{u} = \frac{v_{\parallel o}}{u} + \frac{\delta x}{x_o} + \tfrac{1}{2}\left(\frac{\delta x}{x_o}\right)^2 \quad . \tag{3.6}$$

By inserting this expression into Eq. (2.15) and integrating once again, a relation between δx and $\delta\Phi$ is obtained, namely

$$\tfrac{1}{4}\left(\frac{\delta x}{x_o}\right)^4 + \left(\frac{\delta x}{x_o}\right)^3 + \left(1+\frac{v_{\parallel o}}{u}\right)\left(\frac{\delta x}{x_o}\right)^2 + 2\left(\frac{v_{\parallel o} - v_{\phi o}}{u}\right)\left(\frac{\delta x}{x_o}\right) + \frac{e\delta\Phi}{\frac{1}{2}mu^2} = 0 \tag{3.7}$$

where

$$v_{\phi o} \equiv \frac{\omega}{k_{\parallel o}}$$

and

$$k_{\parallel o} \equiv k_\parallel(x_o) \quad . \tag{3.8}$$

For each value of θ there is a unique value of $\delta\Phi$ determined by Eq. (2.13). Hence Eqs. (2.13) and (3.7) together determine the particle orbits in the θ-x plane.

The particle orbits obtained from these equations are already quite complicated, despite the rather simple model that was chosen to describe the sheared magnetic field. For each value of θ there may be as many as four distinct values of x. Hence, in the θ-x plane these particle

orbits can have four branches. Whether these branches are connected to form "trapped" orbits, or disjoint, giving several "passing" orbits, is determined by the initial phase variables θ_o , x_o , $v_{\|o}$, and the wave amplitude, Φ_o . Hence, our model is sufficient to describe the dumbbell-shaped orbits that we have observed in our numerical integrations of the equations of motion (see Fig. 3).

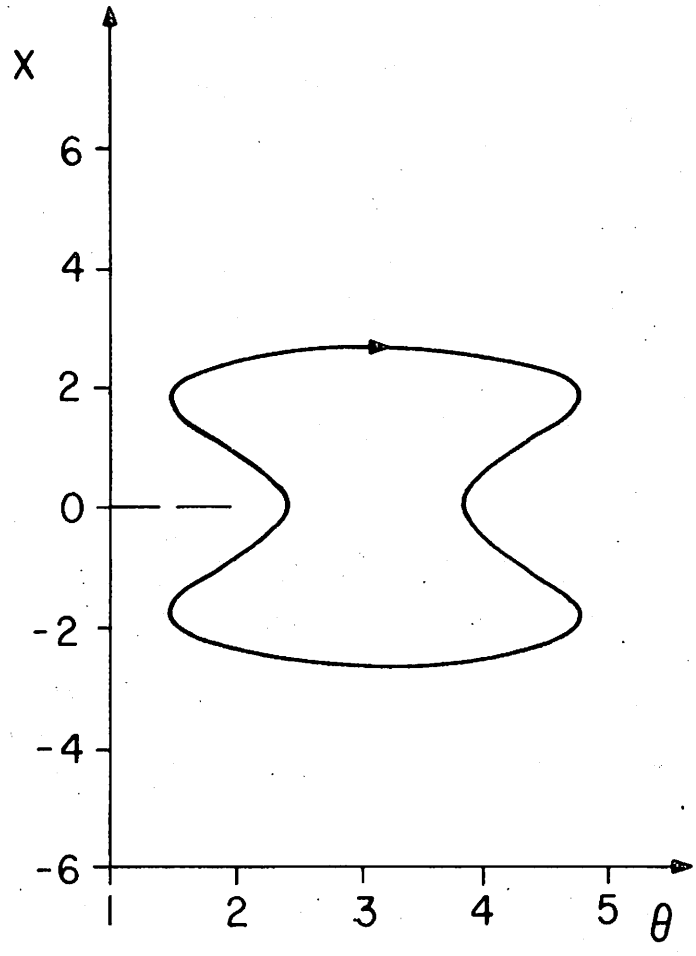

FIGURE 3. Projection of a trapped particle orbit onto the x-θ plane. The "dumbbell" shape results from the change in sign of $k_{\|}$ at $x = 0$.

4. TRAPPED PARTICLE ORBITS

Dumbbell shaped orbits like that shown in Fig. 3 occur when trapped particles cross the $x=0$ plane (where $k_\parallel$ changes sign). In what follows we shall restrict our attention to those particles that remain on one side of this plane. These particles satisfy

$$\frac{\delta x}{x_o} < 1 \ . \tag{4.1}$$

Hence, the cubic and quartic terms in Eq. (3.7) may be neglected in analyzing the orbits of these particles, reducing Eq. (3.7) to the quadratic equation

$$\left(1+\frac{v_{\parallel o}}{u}\right)\left(\frac{\delta x}{x_o}\right)^2 + 2\left(\frac{v_{\parallel o}-v_{\phi o}}{u}\right)\left(\frac{\delta x}{x_o}\right)+\left(\frac{e\delta\Phi}{\frac{1}{2}mu^2}\right)=0 \ . \tag{4.2}$$

Solving this equation for δx in terms of $\delta\Phi$ we obtain

$$\frac{\delta x}{x_o} = \frac{(v_{\parallel o}-v_{\phi o}) \pm d^{\frac{1}{2}}}{(v_{\parallel o}-u)} \ . \tag{4.3}$$

The discriminant, d, is given by

$$d = (v_{\parallel o}-v_{\phi o})^2 - 2\left(1+\frac{v_{\parallel o}}{u}\right)\frac{e}{m}\,\delta\Phi \ . \tag{4.4}$$

Holding the wave amplitude Φ_o constant there is a maximum possible value of $\delta\Phi$, namely

$$\delta\Phi_{max} = \Phi_o - \Phi(t_o) \ . \tag{4.5}$$

Trapped particles oscillate about a minimum of the potential; they do not reach the maximum potential. The turning points of the trapped particle orbits in θ correspond to those values of θ where the two branches of the particle orbit as given by Eq. (4.3) coalesce. This occurs when d vanishes. A criterion for determining if a particle is trapped is obtained by examining this discriminant. For trapped particles the discriminant must vanish for some allowable value of $\delta\Phi$. Hence, d must be negative when evaluated at $\delta\Phi = \delta\Phi_{max}$; and trapped particles must satisfy the condition

$$|v_{\parallel o} - v_{o}| < \left(1 + \frac{v_{\parallel o}}{u}\right)^{\frac{1}{2}} \left(2\frac{e}{m}\delta\Phi_{max}\right)^{\frac{1}{2}} . \tag{4.6}$$

It follows from Eq. (4.6) that the characteristic width of the trapped region in velocity space, v_{TRAP}, is given by

$$v_{TRAP} = (1+\varsigma)^{\frac{1}{2}}(e\Phi_o/m)^{\frac{1}{2}} \tag{4.7}$$

where the parameter ς is defined by

$$\varsigma \equiv \frac{v_{\phi o}}{u} = \frac{v_{\phi o}}{v_{te}} \left(\frac{k}{k_{\parallel o}}\right)^2 \frac{\rho_e}{L_s} . \tag{4.8}$$

In Sect. 6 an estimate of f_p, the fraction of the particles from a given distribution that are trapped by the finite amplitude wave, is required to calculate the pseudoclassical transport coefficients. Assuming that this distribution is nearly Maxwellian, and that both $v_{\phi o}$ and V_{TRAP} are small compared to the thermal velocity v_{te} we may

estimate this fraction as

$$f_p \simeq \frac{v_{TRAP}}{v_{te}} = (1+\varsigma)^{\frac{1}{2}} \left(\frac{e\Phi_o}{T}\right)^{\frac{1}{2}} . \qquad (4.9)$$

In Eq. (4.9) the parameter ς measures the importance of magnetic shear on the trapped particle orbits. If ς is small Eq. (4.9) reduces to the usual estimate (Pogutse, 1972),

$$f_p \simeq \left(\frac{e\Phi_o}{T}\right)^{\frac{1}{2}} . \qquad (4.10)$$

In the oppposite limit, $\varsigma \gg 1$,

$$f_p \simeq \left(\frac{v_{\phi o}}{v_{te}}\right)^{\frac{1}{2}} \left(\frac{\rho_e}{L_s}\right)^{\frac{1}{2}} \left(\frac{k}{k_{\|o}}\right)\left(\frac{e\Phi_o}{T}\right)^{\frac{1}{2}} . \qquad (4.11)$$

This dependence of f_p on parameters other than $(e\Phi_o/T)$ has not appeared previously in the literature. The physical mechanism by which magnetic shear affects particle trapping is described at the end of this section.

Computer simulations were used to check the trapping criterion, Eq. (4.6). The orbits of hundreds of particles were followed in a sheared magnetic field and an electrostatic wave, using the wave form

$$h(\theta) = \cos\theta . \qquad (4.12)$$

It was found that, to within the accuracy of our algorithm for numerical integration, particles initialized with phase variables satisfying

inequality (4.6) execute closed (i.e., trapped) orbits in the θ-x plane, while particles whose initial phase variables do not satisfy inequality (4.6) have open (i.e., passing) orbits. The dependence of f_p on L_s, B, and $k_{\parallel_o}$ predicted by Eq. (4.9) was then verified. A random number generator was employed to select the initial phase variables of hundreds of particles. The parallel velocities were chosen from a Maxwellian distribution, while the initial phase, θ_o, was chosen to be uniformly distributed on $(0,2\pi)$. Inequality (4.6) was used to determine which particles were trapped. The fraction of particles trapped by the wave was computed and compared with our estimate. Fig. 4 shows plots of the computed values of f_p vs. the parameter $\mathcal{S}$. The solid line in this figure corresponds to

$$f_p = 0.37(1 + \mathcal{S})^{\frac{1}{2}}\left(\frac{e\Phi_o}{T}\right)^{\frac{1}{2}} \tag{4.13}$$

where the numerical constant, 0.37, was chosen to give the best fit.

As f_p approaches one the agreement is poor because the assumption that $v_{TRAP} \ll v_{te}$ breaks down. For small values of f_p the statistics are bad. In the intermediate region the agreement between our estimate and the computed value of f_p is excellent. Hence, we conclude that when there is shear in the magnetic field the fraction of particles trapped by a wave can be substantially greater than the usual estimate, $(e\Phi_o/T)^{\frac{1}{2}}$, employed by previous workers (Brambilla and Lichtenberg, 1973; Gell et al., 1975).

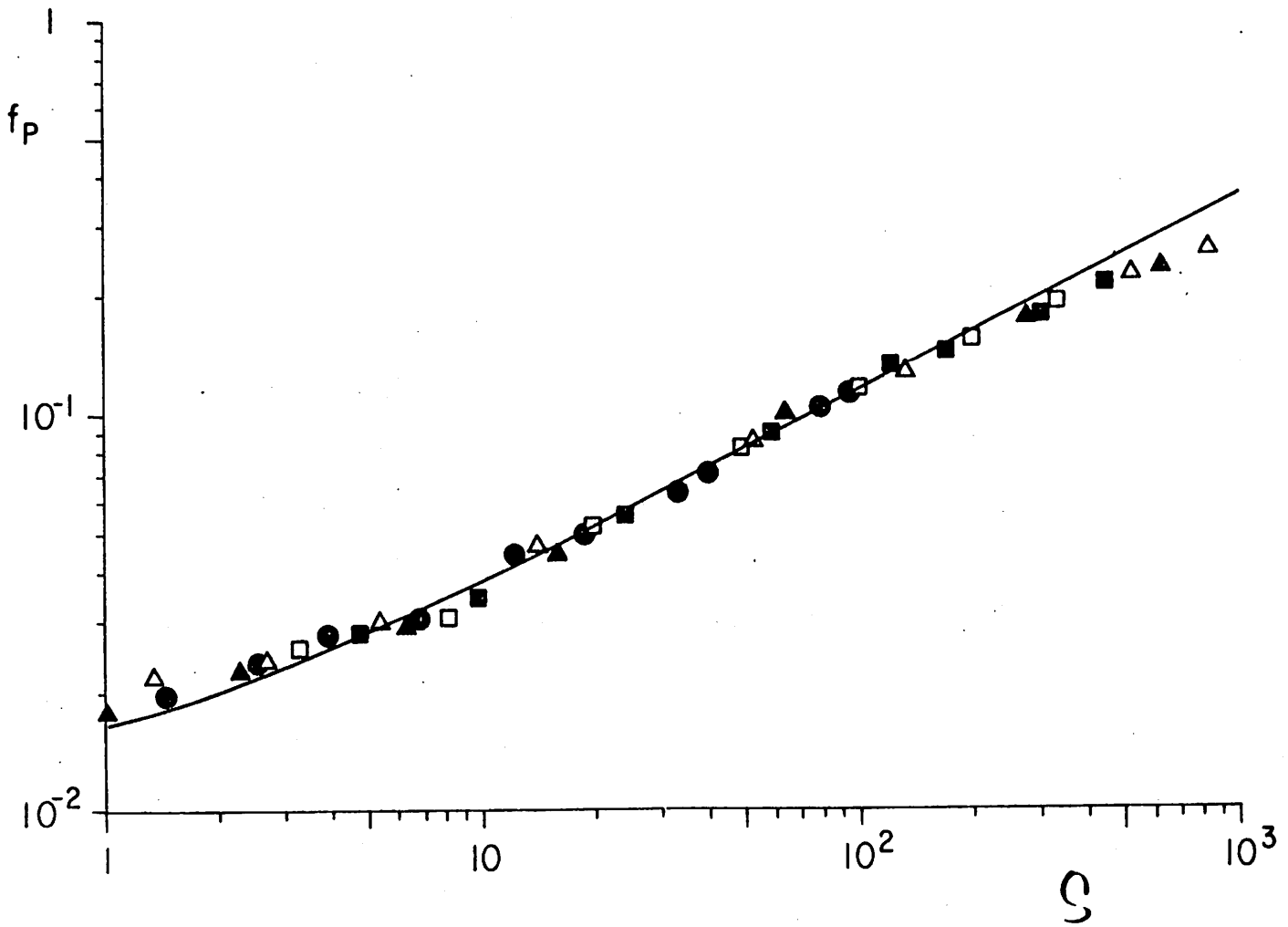

FIGURE 4. This figure illustrates the results of Monte-Carlo calculations of the fraction of particles trapped by the wave, f_p, In these calculations $e\Phi_o/T = .001$ and $v_\phi/v_{te} = 1.414$. For the open square $k_\parallel/k$ and $k\rho_e$ are held constant at .001 and 2.4×10^{-3}, while kL_s is varied. For the solid squares, $k_\parallel/k$ and $k\rho_e$ are fixed at 4.5×10^{-3} and 7.1×10^{-3}. The open triangles illustrate calculations in which $k\rho_e$ and kL_s are held constant at 2.4×10^{-3} and 100. while $k_\parallel/k$ is varied. For the solid triangles $k\rho$ and kLs are given by 7.1×10^{-3} and 100. Finally, the circles show the results of calculations in which $k_\parallel/k$ and kL_s are fixed at .001 and 100. while $k\rho_e$ is varied. The prediction of Eq. (4.13) is shown by the solid line.

Next, we consider the trapped particle orbit widths. Again using the fact that, for trapped particles, t_o may be chosen such that $v_{\|_o} = v_\phi$, and estimating $\delta\Phi_{max}$ by Φ_o, the characteristic orbit width, Δx_p is given by

$$\Delta x_p = \frac{1}{(1+\mathcal{S})^{\frac{1}{2}}} \frac{k}{k_{\|_o}} \sqrt{\frac{e\Phi_o}{T}}\, \rho_e \quad . \tag{4.14}$$

In the limit $\mathcal{S} < 1$ this result is identical to that of Pogutse (1972),

$$\Delta x_p = \frac{k}{k_\|} \left(\frac{e_{\Phi o}}{T}\right)^{\frac{1}{2}} \rho_e \tag{4.15}$$

while when $\mathcal{S}$ is large it goes over to the orbit width of Brambilla and Lichtenberg (1973), namely

$$\Delta x_p = \frac{1}{\mathcal{S}^{\frac{1}{2}}} \frac{k}{k_\|} \left(\frac{e_{\Phi o}}{T}\right)^{\frac{1}{2}} \rho_e \quad . \tag{4.16}$$

Hence, shear in the magnetic field limits the width of the trapped particle orbits when $\mathcal{S} > 1$.

We have estimated the value of $\mathcal{S}$, using values of ω/Ω, $\underline{k}$, and L_s corresponding to the low frequency drift wave spectrum observed in tokamak plasmas. Both large and small values of $\mathcal{S}$ are accessible with reasonable choices of these parameters.

In general, one finds a region about the mode rational surface with a width

$$x_S \equiv \left\{ \frac{\omega}{\Omega_e} \frac{L_s^2}{k} \right\}^{1/3}$$

$$\simeq \rho_i \left\{ \frac{m_e}{m_i} \frac{L_s^2}{\rho_i L_n} \right\}^{1/3} \qquad (4.17)$$

in which ς is greater than one. Outside of this region ς is less than one, and the effect of magnetic shear on the trapped particle orbits may be neglected. In writing the second of Eqs. (4.17) we have estimated ω by the electron diamagnetic drift frequency. L_n is the density gradient scale length. Using parameters characteristic of the drift wave spectra observed in a tokamak plasma we find that x_S is of the same order of magnitude as the ion gyro-radius, ρ_i. Since the radial mode structure of the low frequency drift wave is a subject of current research (see, e.g., Renwoldt et al., 1977; Ross et al., 1977; Smith and Whitson, 1977; Miner and Ross, 1977), it is not yet clear whether the normal modes are localized in the region in which $\varsigma > 1$, or extend into the region in which $\varsigma < 1$. Hence, it is necessary to consider both large and small values of ς in determining the enhanced transport associated with the trapping of particles by the drift wave spectrum.

In the preceding analysis of the orbits of particles trapped by an electrostatic wave in a sheared magnetic field time was eliminated as an independent variable. We must now return to the equations of motion to determine the time scale associated with these trapped particle oscillations. This time scale is determined by ω_{BOUNCE}, the bounce frequency of a deeply trapped particle.

It is convenient to assume that the waveform, $h(\theta)$, is given by

$$h(\theta) = - \cos \theta \tag{4.18}$$

and examine the orbits of particles trapped about $\theta = 0$. By linearizing Eq. (2.6), one obtains

$$\frac{d\theta}{dt} = k_{\parallel o}\delta v + v_{\parallel o}\delta k \tag{4.19}$$

where $\delta k_{\parallel} \equiv k(\delta x/L_s)$. Equation (3.4) is used to eliminate $\delta v_{\parallel}$ from Eq. (4.19), leaving

$$\frac{d\theta}{dt} = \frac{ku}{L_s}(1 + \mathcal{S})\ \delta x \tag{4.20}$$

where t_o is chosen such that $v_{\parallel o} = v_{\phi o}$. Taking the time derivative of Eq. (4.20), and using Eq. (2.5) to express $d\delta x/dt$ in terms of θ, it is found that

$$\frac{d^2\theta}{dt^2} = -k_{\parallel o}^2 (1 + \mathcal{S}) \frac{e}{m} \Phi_o\, h'(\theta)\ . \tag{4.21}$$

For deeply trapped particles θ is small, so $h'(0)$ may be expanded to obtain

$$\frac{d^2\theta}{dt^2} = - \omega_{BOUNCE}^2\, \theta \tag{4.22}$$

where

$$\omega_{BOUNCE} = k_{\parallel o} v_{te} (1 + \mathcal{S})^{\frac{1}{2}} \left(\frac{e\Phi_o}{T}\right)^{\frac{1}{2}}\ . \tag{4.23}$$

Hence, the bounce frequency of the trapped particles depends on the shear in the magnetic field only through the parameter S, and magnetic shear tends to increase the bounce frequency of the electrostatically trapped particles.

It is interesting to note that if only the first term on the right hand side of Eq. (4.19), $k_{\|o}\delta v_{\|}$, is retained, then one recovers the shearless result, $\omega_{BOUNCE} = k_{\|o}\sqrt{e\phi_o/m}$. The remaining term, $v_{\|o}\delta k_{\|}$, gives rise to the dependence of ω_{BOUNCE} on S. In the limit of large S this second term dominates Eq. (4.19). Hence, we see that shear affects the particle orbits through the variation in $k_{\|}$. This variation is caused by the E×B drift of the particle across the sheared magentic field. An observer moving with the particle would see the wave slowing down as he moved in the direction of increasing $k_{\|}$; while the phase velocity of the wave would increase as he moved in the direction of decreasing $k_{\|}$. Hence, when this second term dominates Eq. (4.19), the oscillation of the particle between the maxima of the wave potential occurs due to the variation in the local phase velocity of the wave, $\omega/k_{\|}(x)$. This is in sharp contrast to the trapping mechanism in a magnetic field with no shear (i.e., $S = 0$), where it is the velocity of the trapped particle that varies, rather than the phase velocity of the wave.

5. THE TRANSPORT COEFFICIENTS

In the preceding sections the orbits of particles trapped by an electrostatic wave in a sheared magnetic field (pineapple orbits) were examined. Estimates of the pineapple orbit width, Δx_p, the width of the trapped region in velocity space, v_{TRAP}, the fraction of particles from a thermal distribution that are trapped by a given wave, f_p, and the bounce frequency of a deeply trapped particle, ω_{BOUNCE}, were obtained. In this section these estimates will be employed together with a random walk model to determine the scaling of the anomalous transport driven by an electrostatic wave with ω, $\underline{k}$, and $(e\Phi_o/T)$, given ν_e, B, and L_s.

When a random walk model is used to estimate transport coefficents it is often helpful to divide velocity space into two regions such that particles in the different regions have qualitatively different orbits. Collisions will cause particles to "jump" from one region of velocity space to the other. The accompanying change in the character of the particle orbit produces a "step" across the magnetic field. This division of velocity space has been used in estimates of the neoclassical transport coefficients (e.g., Dean et al., 1974; Stringer, 1970) and in previous treatments of pseudoclassical transport theory (e.g., Pogutse, 1972; Brambilla and Lichtenberg, 1973; Gell et al., 1975).

In the limit of small collision frequency, velocity space may be divided into a region in which particles are trapped in the electric field of the wave and a region of passing orbits. In these two regions the particle orbits are qualitatively different. The trapped particles

see a slowly varying electric field, and consequently their orbits are extended in the x-direction. These are the "pineapple" orbits analyzed in Section 4.

A typical passing particle experiences a rapidly varying electric field, and consequently "jitters" about its mean position with an amplitude*

$$\Delta x \sim \left(\frac{k}{k_\parallel}\right)\left(\frac{e\Phi}{T}\right)\rho_e \tag{5.1}$$

which is small compared to the pineapple orbit width, Δx_p .

Collisions cause particles to be scattered in and out of the trapped region of phase space. Each time this occurs the mean particle position is displaced in x . The characteristic size of this displacement is the pineapple orbit width, Δx_p , given by Eq. (4.14). Viewing this process as a random walk, we obtain a diffusion coefficient,

$$\mathcal{D} = \alpha f_p \Delta x_p^2 \nu_{eff} \tag{5.2}$$

where f_p is the fraction of velocity space occupied by trapped particles, ν_{eff} is the effective collision frequency for scattering in or out of the trapped region, and α is a numerical coefficient of order unity.

The effective collision frequency is greater than ν_e , the frequency at which many small angle collisions accumulate to produce a 90° scattering angle, because trapped electrons become untrapped when scattered through an angle $\Delta\theta \simeq (v_{TRAP}/v_{te})$. Since small angle scattering

*This result follows directly from Eq. (4.2) when $v_{\parallel o}-v_\phi$ is esimated by v_{te} .

is the dominate collisional process in fully ionized plasmas, the effective collision frequency is related to the 90° collision frequency by

$$\nu_{eff} = \frac{1}{(\Delta\theta)^2}\nu_e = \frac{\nu_e}{(1+\mathcal{S})(e\Phi/T)} \quad . \tag{5.3}$$

The plasma-wave system is in the "pineapple" regime when the collision frequency is small enough that trapped particles typically complete a bounce orbit in the wave potential before being scattered out of the trapped region. This is the case when

$$\frac{\nu_{eff}}{\omega_{BOUNCE}} \ll 1 \quad . \tag{5.4}$$

or equivalently,

$$\nu_* \equiv \frac{\nu_e}{k_\parallel v_{te}} \ll \left[\left(\frac{e\Phi}{T}\right)(1+\mathcal{S})\right]^{3/2} \quad . \tag{5.5}$$

In this limit Eq. (5.2) predicts that the transport coefficients will be proportional to

$$D_p \equiv (1+\mathcal{S})^{-3/2}\left(\frac{e\phi}{T}\right)^{1/2}\left(\frac{k}{k_\parallel}\right)^2 \rho_e^{\,2}\,\nu_e \quad . \tag{5.6}$$

Hence, the particle diffusion coefficient, $\mathcal{D}$, may be written in the form

$$\mathcal{D} = \alpha D_p \tag{5.7}$$

while the heat conductivity

$$\chi = \beta D_p \quad . \tag{5.8}$$

Similar expressions apply for the off-diagonal transport coefficients. While we expect that the constants of proportionality, α and β, are of order unity, the numerical values of these constants must be obtained from kinetic theory.

A kinetic calculation of the pseudoclassical transport coefficients was performed in the limit $\varsigma = 0$ (Nevins, 1977a). This calculation may be extended to sheared magnetic fields by requiring that the dependence of the transport coefficients on ς be given by Eq. (5.6), and that the known values of the transport coefficients are recovered in the limit $\varsigma = 0$. Hence, in a sheared magnetic field the pseudoclassical particle and energy fluxes are given by the results of Nevins together with our more general D_p,

$$\Gamma_e = -2.25\, D_p \left(1 - \frac{\omega}{\omega_{ne}}\right) \frac{\partial n}{\partial x} + 1.89\, D_p \frac{n}{T} \frac{\partial T}{\partial x} \qquad (5.9)$$

$$Q_e = -1.48\, D_p \left(1 - \frac{\omega}{\omega_{ne}}\right) T \frac{\partial n}{\partial x} + 0.23\, D_p\, n \frac{\partial T}{\partial x} \quad . \qquad (5.10)$$

ω_{ne} is the electron diamagnetic drift frequency,

$$\omega_{ne} \equiv - \frac{k_y T}{eB} \frac{1}{n} \frac{\partial n}{\partial x} \quad . \qquad (5.11)$$

The wave frequency appears explicitly in Eqs. (5.9)-(5.10) because the thermodynamic forces on the wave-plasma system are

$$A_1 = \left(1 - \frac{\omega}{\omega_{ne}}\right) \frac{1}{n} \frac{\partial n}{\partial x} - \frac{3}{2} \frac{1}{T} \frac{\partial T}{\partial x} \tag{5.12}$$

$$A_2 = - \frac{1}{T} \frac{\partial T}{\partial x} \quad . \tag{5.13}$$

Hence, the factor $(1-\omega/\omega_{ne})$ is <u>not</u> part of the transport coefficient, but is instead part of the thermodynamic force (Nevins, 1977a,c).

In the computer simulations of pseudoclassical transport presented in Sect. 7 only the electron-ion collisions are retained. Nevins (1977a) showed that the contribution of electron-ion collisions to the pseudoclassical electron diffusion coefficient, $\mathcal{D}^{e-i}$, is

$$\mathcal{D}^{e-i} = 1.30\ D_p \ . \tag{5.14}$$

This result is found to be in good agreement with the computer simulations.

Next, in the intermediate regime of collision frequencies,

$$\left[\left(\frac{e\Phi_o}{T}\right)(1+\mathcal{S})\right]^{3/2} \ll \nu_* \ll 1 \ , \tag{5.15}$$

particles are no longer trapped by the wave. The particles are detrapped by collisions before they can complete a full "pineapple" orbit. The pseudoclassical transport coefficients in this regime are estimated by adapting Stringer's (1970) explanation of the neoclassical plateau regime. At intermediate values of the collision frequency the particle velocity space may still be divided into two regions, a "resonant" region and a "non-resonant" region. The "resonant" region of velocity space is defined to be that region in which the Doppler shifted wave frequency, $\omega - k_\parallel v_\parallel$, is less than the effective collision frequency for scattering particles out of the resonant region of velocity space, ν_{res} . Between collisions resonant particles drift across the magnetic field with a velocity of order $v_E = k\Phi_o/B$. The remainder of velocity space is the non-resonant region. Between collisions non-resonant particles jitter back and forth across the magnetic field. Hence, the orbits of resonant and non-resonant are qualitatively different.

The width of the resonant region in velocity space, v_{res}, is given by equating the Doppler shifted wave frequency on the boundary of the resonant region to ν_{res}, i.e.,

$$k_{\parallel} v_{res} = \nu_e \left(\frac{v_{te}}{v_{res}} \right)^2 . \tag{5.16}$$

or

$$v_{res}/v_{te} = (\nu_*)^{1/3} . \tag{5.17}$$

Hence,

$$\nu_{res} = \nu_e \nu_*^{-2/3} . \tag{5.18}$$

Just as before, the diffusion coefficient is given by

$$D_{res} = f_{res} \Delta x_{res}^2 \nu_{res} . \tag{5.19}$$

For waves with phase velocities, $v_\phi = \omega/k_{\parallel}$, small compared to the electron thermal velocity, the fraction of the electrons resonant with the wave is

$$f_{res} = \frac{v_{res}}{v_{te}} \tag{5.20}$$

while the step size of the resonant particles is given by

$$\Delta x_{res} = \frac{k\phi_o}{B} \frac{1}{\nu_{res}} . \tag{5.21}$$

Hence, we may estimate the diffusion coefficient by

$$D_{res} = \frac{1}{k_{\parallel} v_{te}} \frac{k^2 \phi_o^2}{B^2} \quad . \tag{5.22}$$

This estimate of the particle diffusion coefficient, D_{res}, differs from the self-consistent diffusion coefficient (see, e.g., Sagdeev and Galeev, 1969; Horton, 1976; Krall and McBride, 1977),

$$\mathcal{D}_{sc} = (\pi/8)^{\frac{1}{2}} \frac{1}{k_{\parallel} v_{te}} \frac{k^2 \phi_o^2}{B^2} \tag{5.23}$$

only by the numerical factor, $(\pi/8)^{\frac{1}{2}}$. The relation between the collisional transport process described here, and the self-consistent transport investigated by other authors has been considered elsewhere (Nevins, 1977b) with the conclusion that the transport will be properly described by the self-consistent theory when inequality (5.15) is satisfied. This result is confirmed by the computer simulations presented in the next section.

The "self-consistent" transport coefficients are called "quasilinear" transport coefficients by some authors (e.g., Sagdeev and Galeev, 1969; Krall and McBride, 1977). The name "self-consistent" is used here to emphasize the fact that it is <u>not</u> necessary to make any assumptions about the auto-correlation time of the wave spectrum in deriving these transport coefficients (see, e.g., the derivations of Horton, 1976; Liu, et al., 1976; Manheimer, 1977). The self-consistent transport coefficients simply describe the transport of particles and energy implied by the linear perturbation in the electron distribution function. Hence,

it is not unreasonable to apply these transport coefficients in calculating the transport due to a single, coherent wave.

Finally, the collisional limit,

$$\nu_* > 1 \ , \tag{5.24}$$

of pseudoclassical transport theory is investigated. This regime was treated previously by Yoskikawa and Christofolis (1971) using fluid theory. Here we present an alternate derivation of the same diffusion coefficient. In the collisional limit particles are no longer free to stream along the magnetic field lines. Instead, the parallel motion must be viewed as a random walk, with a characteristic step size

$$\Delta z = \frac{v_{te}}{\nu_e} \ . \tag{5.25}$$

Hence, a typical particle will be displaced by a distance of order $1/k_\parallel$ along the magnetic field in a time

$$t_\parallel = \frac{\nu_e}{k_\parallel^2 v_{te}^2} \ . \tag{5.26}$$

In the limit

$$\omega t_\parallel \ll 1 \ , \tag{5.27}$$

the electric field seen by the particles changes primarily due to the diffusion of particles parallel to the magnetic field.

Viewing the motion of the particle across the magnetic field as a random walk, we take the step size to be

$$\Delta x_c = \frac{k_\perp \Phi_o}{B} \; t_\parallel \tag{5.28}$$

and the correlation time to be $t_\parallel$. Hence, the diffusion coefficient that describes the motion of particles across the magnetic field in the colllsional limit is given by

$$D_c = \frac{\nu_e}{k_\parallel^2 v_{te}^2} \frac{k_\perp^2 \Phi_o^2}{B^2} \; . \tag{5.29}$$

6. RESULTS OF COMPUTER SIMULATIONS

In this section we present the results of computer simulations of the pseudoclassical transport process. The computer code constructed for these simulations is described in Appendix B. The plan of attack will be to first compare the particle transport rates that we observe in these computer simulations with the predictions of the kinetic theory of pseudoclassical transport (Nevins, 1977a) in the limit of no magnetic shear, $S = 0$. Next, we shall investigate the dependence of the transport coefficients on the amount of shear in the magnetic field, and, finally, compare the observed transport rates with the predictions of Section 6 in the limit of strong magnetic shear, $S \gg 1$.

The computer simulation code measures D^* , the enhancement in the electron diffusion coefficient over its classical value due to the presence of the finite amplitude wave. These measurements of D^* are consistent with the results of kinetic theory in the limit of vanishing magnetic shear. Figure 5 shows D^* versus the collision frequency. At small collision frequencies, when $(\nu_{eff}/\omega_{BOUNCE}) \lesssim .1$, the measured diffusion rates, D^* , are in very good agreement with the pseudoclassical diffusion coefficient calculated by Nevins (1977a) (indicated by the solid line). This close agreement between the computer simulations and kinetic theory is particularly significant in light of the fact that there are no free parameters in this theory. As $(\nu_{eff}/\omega_{BOUNCE})$ approaches one the measured diffusion coefficient departs from the theoretical prediction. The discrepancy, which is of order $(\nu_{eff}/\omega_{BOUNCE}) \cdot D_p$, is expected as terms of this order were ignored in the kinetic calculation.

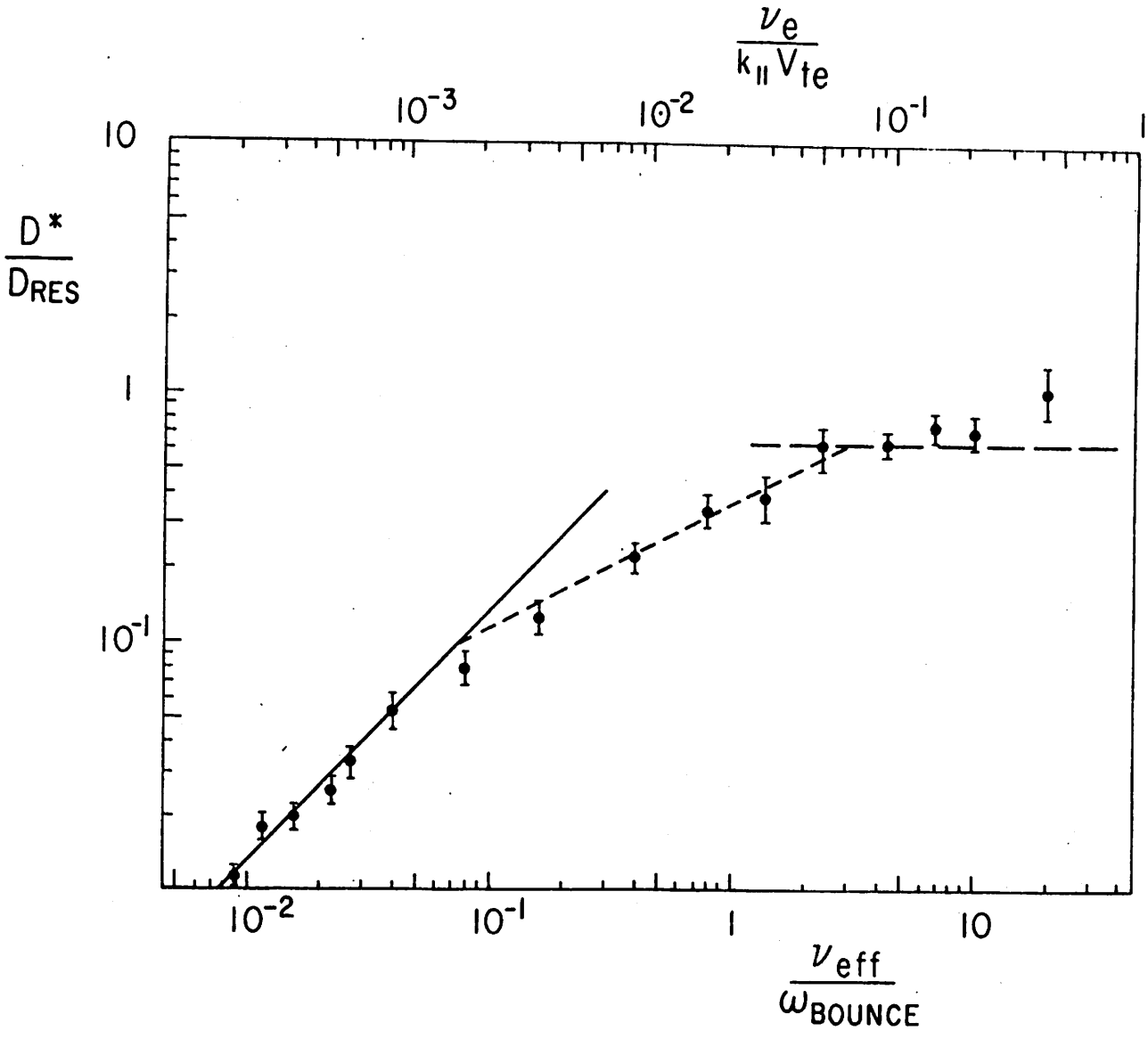

FIGURE 5. Measured values of the enhancement in the diffusion coefficient versus the collision frequency. The prediction of Eq. (5.14) is shown by the solid line. The dotted line corresponds to $D^* = 2.4\nu_*^{\frac{1}{2}} D_{res}$, where the constant factor, 2.4, has been chosen to fit the data. The dashed line shows the self-consistent diffusion rate given by Eq. (5.23). $(e\Phi_o/T)$, $k_\parallel/k$, v_ϕ/v_{te}, and $k\rho_e$ were held constant at .08, 0.2, 0.0, and 4.3×10^{-3}, respectively. The vertical error bars here represent fluctuations in D^*.

When the collision frequency is in the intermediate range,

$$.1 \leq (\nu_{eff}/\omega_{BOUNCE}) \leq 2 \qquad (6.1)$$

the computer simulations show a transition regime in which the enhanced transport scales as the square root of the collision frequency, i.e.,

$$\mathcal{D}^{e-i} \simeq 2.4\ \nu_*^{\frac{1}{2}}\ D_{res}\ . \qquad (6.2)$$

We are unaware of any calculation of the pseudoclassical transport coefficients from kinetic theory that is valid in this regime. However, the close analogy between the neoclassical and pseudoclassical transport mechanisms suggests that the behavior of the pseudocalssical transport coefficients should be similar to that of the neoclassical transport coefficients. The values of the neoclassical transport coefficients over the analogous transition from the neoclassical "banana" regime to the neoclassical "plateau" regime have been worked out in detail (see, e.g., Hinton and Hazeltine, 1976). This kinetic calculation predicts a broad transition regime in which the transport coefficients are proportional to $\nu_*^{\frac{1}{2}}$. Hence, this analogy leads one to expect exactly the $\nu_*^{\frac{1}{2}}$ scaling observed in Fig. 5.

At higher values of the collision frequency the transition regime is followed by a plateau in which the enhanced diffusion rates are nearly independent of the collision frequency. Figure 5 shows that the measurements of D^* on the plateau are well approximated by the "self-consistent" diffusion coefficient discussed in Sect. 5, Eq. (5.23). Hence, these simulations provide strong support for our identification of the plateau regime of pseudoclassical transport with the self-consistent transport considered by many other authors (e.g., Stix, 1967; Sagdeev and Galeev, 1969; Horton, 1976).

Finally, when $\nu_* \sim 1$, the transition to the "collisional" regime of pseudoclassical transport begins to appear (Yoshikawa and Christofolis, 1971). We did not proceed to larger collision frequencies in this sequence of computer simulations because, for the particular choice of parameters made in these simulations the enhancement in the particle diffusion in the collisional regime over the classical rate (Rosenbluth and Kaufman, 1958),

$$D_{cl} = \rho_e^2 \nu_e \ , \tag{6.3}$$

is too small to be measured. Of course, this is not always the case; in fact at values of $k_\parallel/k$ smaller than those used in Fig. 5, the pseudoclassical transport rates in the collisional regime can be substantially larger than the classical transport rates. We conclude this discussion of Fig. 5 by noting that, in the limit of vanishing magnetic shear, pseudoclassical transport theory describes the observed enhancement in the electron transport rate over a wide range of collision frequencies.

We now restrict our attention to the low collision frequency, or "pineapple" regime. Fig. 6 illustrates the results of computer simulations which verify the scaling of D^* in the pineapple regime with $k_\parallel/k$ predicted by Eq. (5.5). The solid line is the prediction of the kinetic theory, as given by Eq. (5.14). The observed values of D^* are in excellent agreement with the kinetic theory. The scaling of D^* with the magnetic field strength, B, has been verified elsewhere (Gell, et al., 1975).

In Fig. 7 the measured enhancement in the diffusion coefficient is plotted against $(e\Phi_o/T)$. These results are in good agreement with the kinetic theory of pseudoclassical transport for $(e\Phi_o/T) \lesssim 0.25$. It is somewhat surprising that the kinetic theory properly describes the pseudoclassical transport at such large values of the wave amplitude, as terms of order $(e\Phi_o/T)^{\frac{1}{2}}D_p$ were ignored in the kinetic theory.

We conclude our examination of pseudoclassical transport in the limit of vanishing magnetic shear by investigating the dependence of D^* on the phase velocity of the finite amplitude wave. In both the kinetic theory of Nevins (1977) and the estimates of the pseudoclassical transport rates presented above, terms involving $(v_\phi/v_{te})^2$ were ignored. We expect that the pseudoclassical transport coefficients will drop off as (v_ϕ/v_{te}) is increased, for two reasons. First, there will be fewer particles trapped by the wave because the distribution function decreases with increasing velocity. In addition, the average speed of the resonant particles,

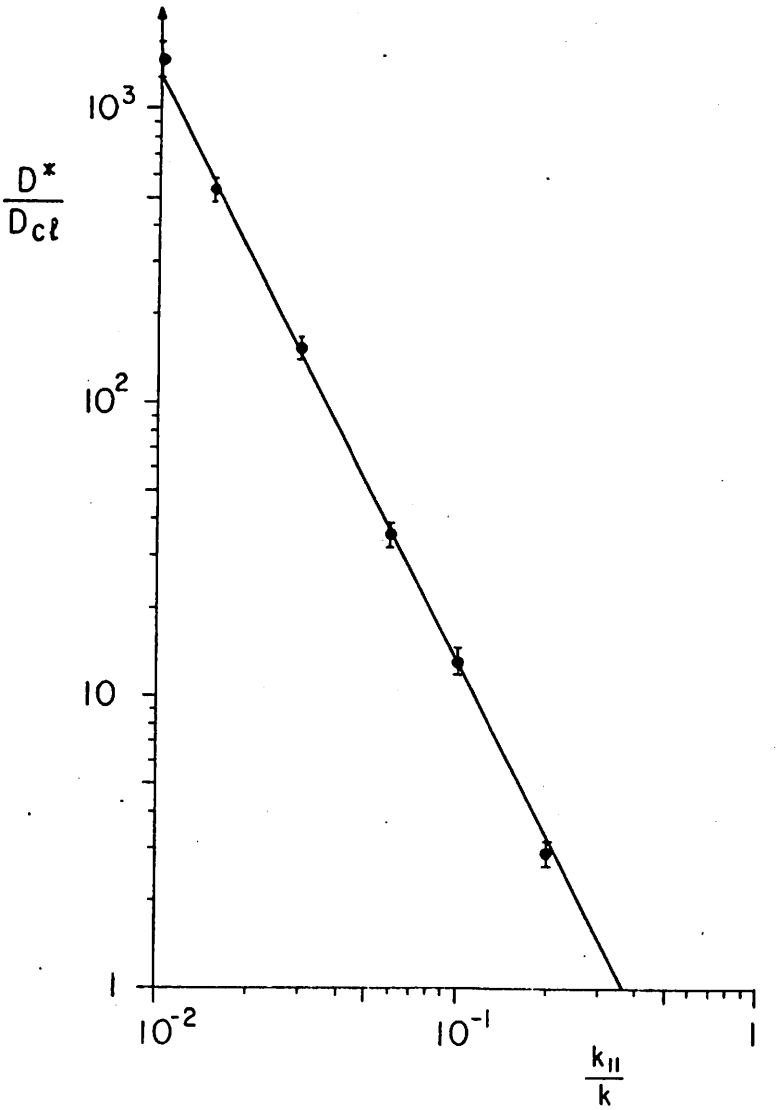

FIGURE 6. Measured values of the diffusion coefficient versus $k_{\|}/k$, with D* normalized to the classical diffusion rate. The prediction of Eq. (5.14) is shown by the solid line. $(e\Phi_o/T)$, $k\rho_e$, v_ϕ/v_{te}, and $(\nu_{eff}/\omega_{BOUNCE})$ were held constant at .01, 4.3×10^{-3}, 0.0, and 0.5, respectively.

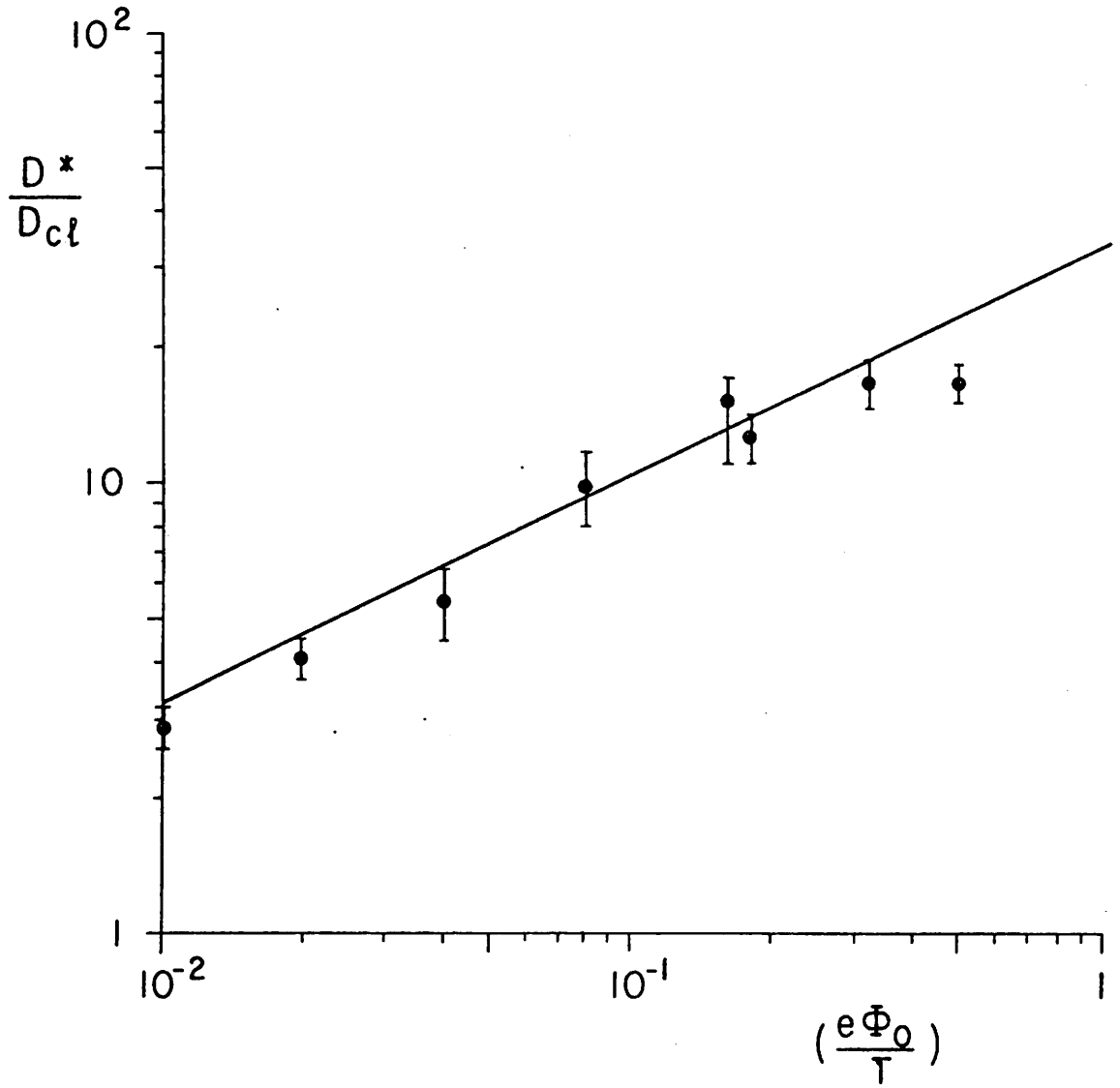

FIGURE 7. Measured enhancement in the diffusion coefficient versus $(e\Phi_o/T)$. The prediction of Eq. (5.14) is shown by the solid line. $k_\parallel/k$, and $v_{\phi o}/v_{te}$ are held fixed at 0.2 and 0.0, respectively, while $(\nu_{eff}/\omega_{BOUNCE}) = 5.0 \times 10^{-2}$. The dependence on B is scaled out because D* is normalized to D_{cl} .

$$\bar{v} \simeq (v_\phi^2 + v_{te}^2)^{1/2}$$

increases with v_ϕ . Since the electron-ion collision frequency varies as $1/v^3$, the effective collision frequency of the resonant particles will decrease as v_ϕ is increased. Hence, we might expect that

$$\mathcal{D}^{e-i}(v_\phi) \simeq \frac{e^{-v_\phi^2/2v_{te}^2}}{[1+(v_\phi/v_{te})^2]^{3/2}} \mathcal{D}^{e-i}(v_\phi=0) \quad . \tag{6.4}$$

Figure 8 shows the measured diffusion coefficient, D^* , versus (v_ϕ / v_{te}) . When $(v_\phi / v_{te}) \leq .7$ we find qualitative agreement with the Eq. (6.4), shown by the solid line. At larger values of (v_ϕ / v_{te}) , D^* is consistently larger than this estimate.

We now present our measurements of the pseudoclassical diffusion in a sheared magnetic field. We noted previously (c.f., Sect. 4) that shear in the magnetic field is important in limiting the widths of particle orbits near the mode rational surface. In this region the pseudoclassical diffusion coefficient is strongly dependent on position (see Fig. 12). This spatial dependence of the diffusion coefficient causes some difficulty because our computer code in fact averages over a region with a width several times greater than the pineapple orbit width, Δx_p , in its measurement of D^* . Thus, compromises in our choice of simulation parameters were necessary to insure sufficient spatial resolution. We have examined the constraints on our choice of simulation parameters

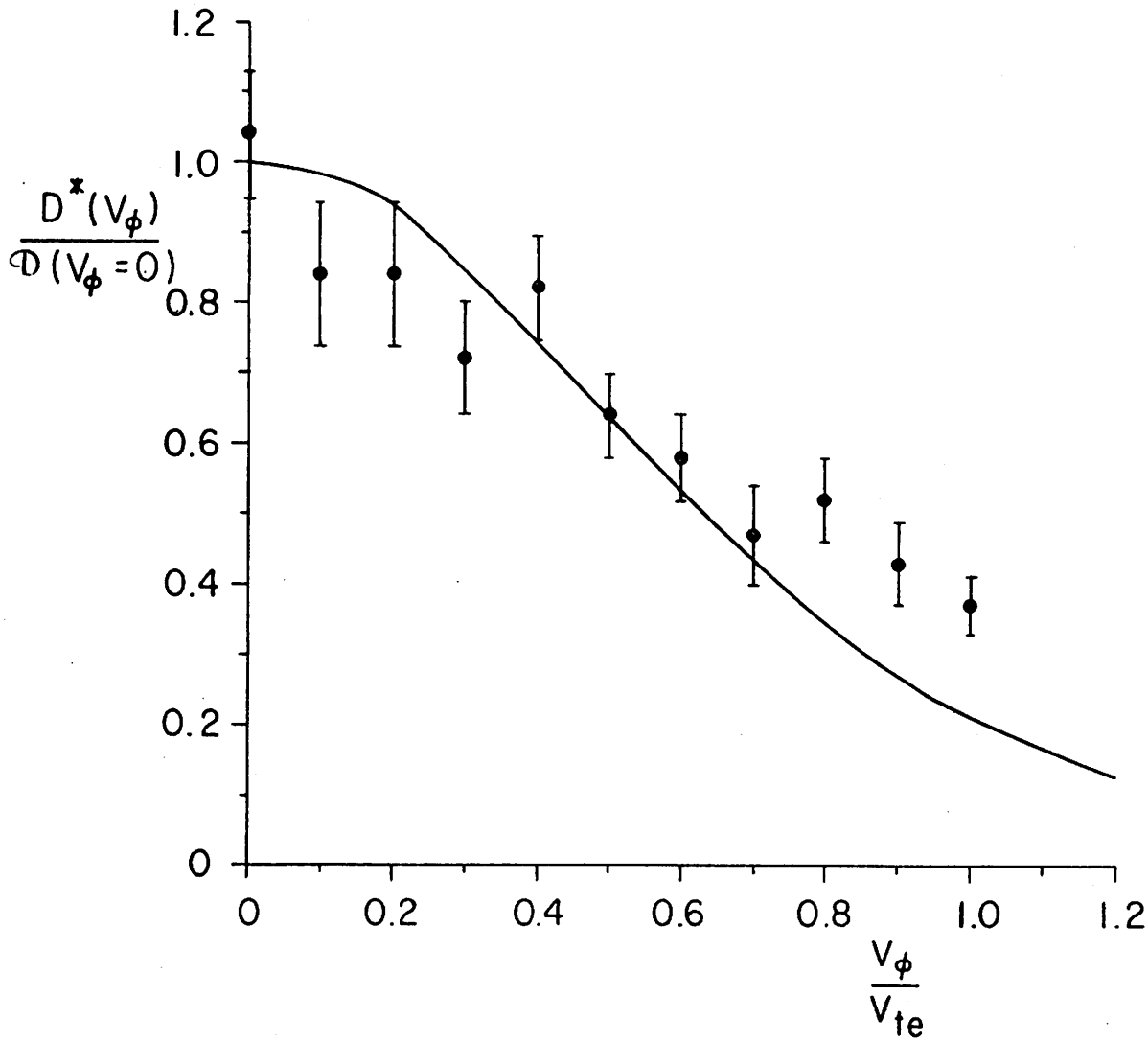

FIGURE 8. D* versus the phase velocity. The solid line corresponds to Eq. (6.4). $(e\Phi_o/T)$, $k_\parallel/k$, $k\rho_e$, and $(\nu_{eff}/\omega_{BOUNCE})$ were held constant at .01, .03, 4.3×10^{-3}, and .05, respectively.

elsewhere (Harte and Nevins, 1976) and concluded that it is necessary to choose the wave frequency such that the local value of the phase velocity is of the same order as the thermal velocity. Hence, we are unable to directly verify the theoretical prediction of Eq. (5.14), as this theory assumes that $v_\phi \ll v_{te}$. We have verified the scaling of D* with $k_\parallel$, L_s , and B predicted by Eq. (5.6).

Figure 9 illustrates the transition between the regimes of small and large magnetic shear. The parameter ς is varied between 0.1 and 10.0 by changing the magnetic shear length, L_s . A continuous transition is observed between the limit of small and large shear in which the diffusion coefficient scales as $(1+\varsigma)^{-3/2}$, which is predicted by Eq. (5.6). The solid line is the theoretical prediction of Eq. (5.14) together with Eq. (5.6), corrected by the factor 0.6 to allow for the rather large value of $(v_{\phi o}/v_{te})$ employed in these computer simulations, $(v_{\phi o}/v_{te}) = 0.5$. The magnitude of this correction factor is made plausible by both Eq. (6.4) and Fig. 8.

Figure 10 illustrates the dependence of D* on the collision frequency in the strongly sheared limit. The dependnece is linear at small values of $(\nu_{eff}/\omega_{BOUNCE})$, as our theory predicts. This linear dependence breaks down at somewhat lower values of $(\nu_{eff}/\omega_{BOUNCE})$ than we would have expected.

Finally, Figure 11 illustrates a series of computer simulations in which L_s , $\underline{B}$, and $k_\parallel/k$ were varied independently. The solid line shows the prediction of Eq. (5.14). For values of ς up to forty the measured diffusion rates fall below the prediction of Eq. (5.14)

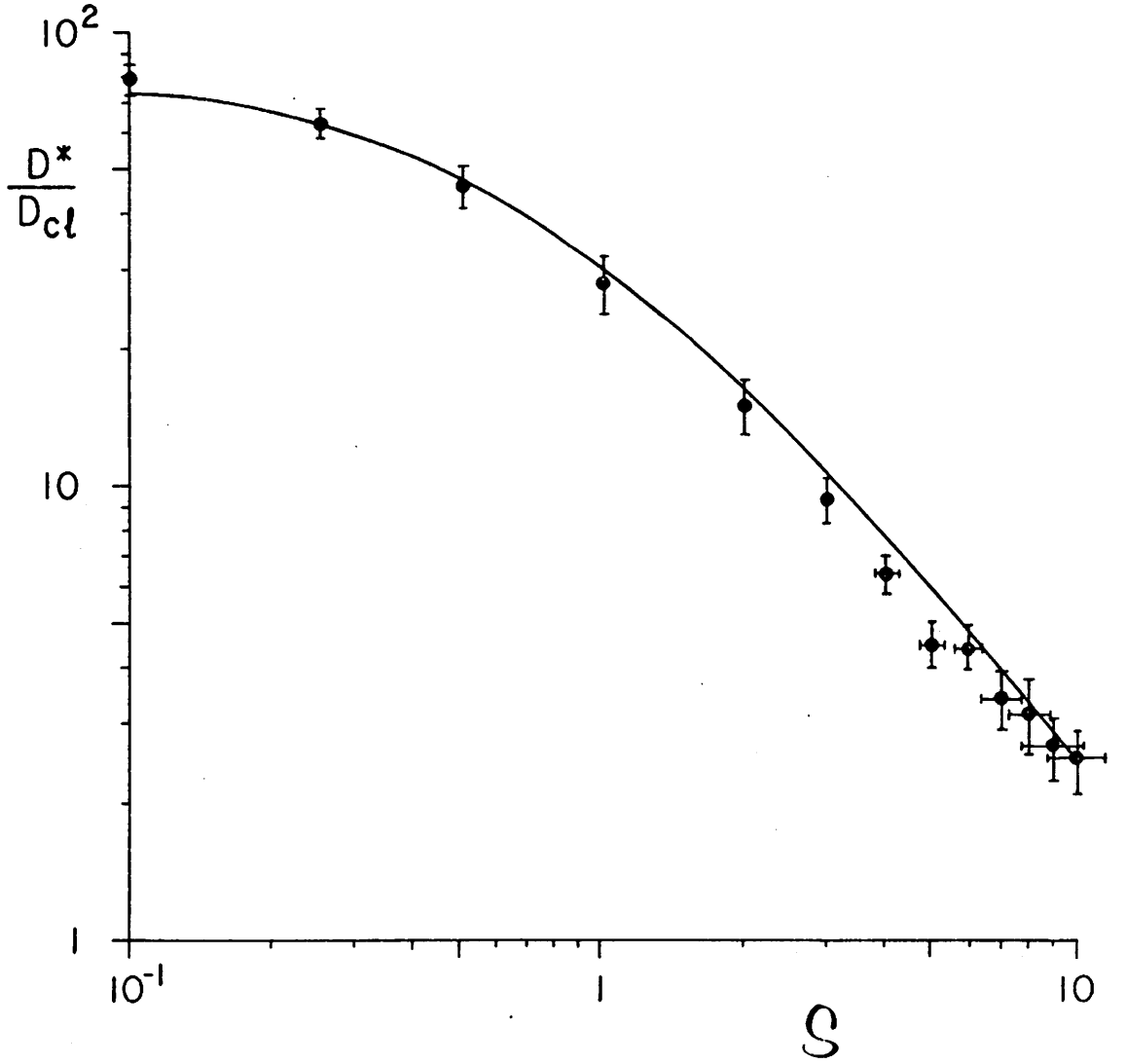

FIGURE 9. D* normalized to D_{cl} versus ς, showing the transition between the regimes of small and large shear. $(e\Phi_o/T)$, $k_\parallel/k$, $v_{\phi o}/v_{te}$, and $k\rho_e$ are held constant at .01, .03, 0.5, and 4.3 10^{-3}, respectively, while kL_s is varied. The solid line is $0.6 \cdot \mathcal{D}^{e-i}$ of Eq. (5.14). The horizontal error bars reflect the finite spatial resolution of the measured diffusion coefficient, D*.

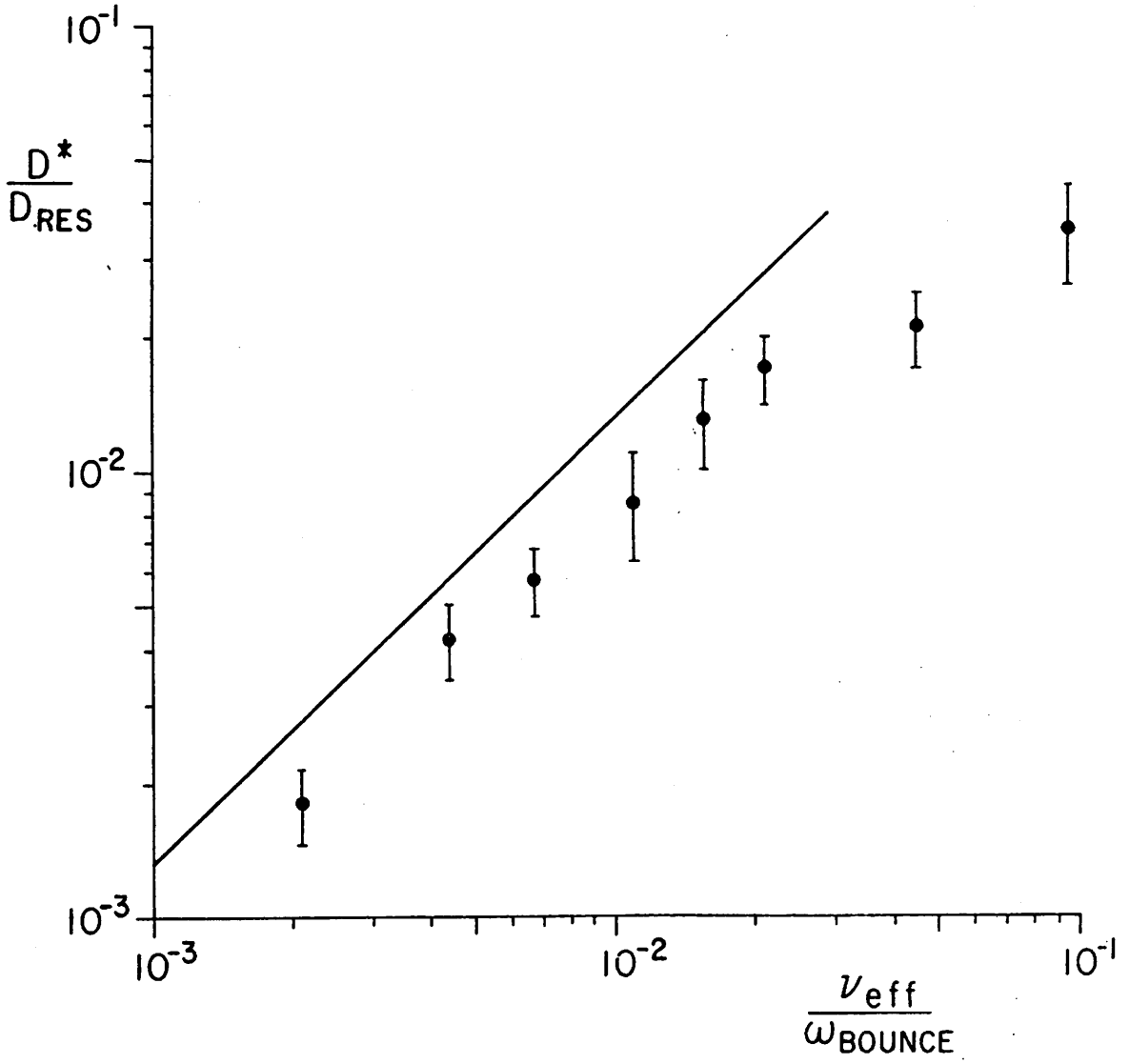

FIGURE 10. D* versus the collision frequency. $(e\Phi_o/T)$, $k_\parallel/k$, $v_{\phi o}/v_{te}$, and $k\rho_e$ are held constant at .001, .001, 1.414, and 2.4 10^{-3}, respectively, while the collision frequency is varied. The prediction of Eq. (5.14) is shown by the solid line.

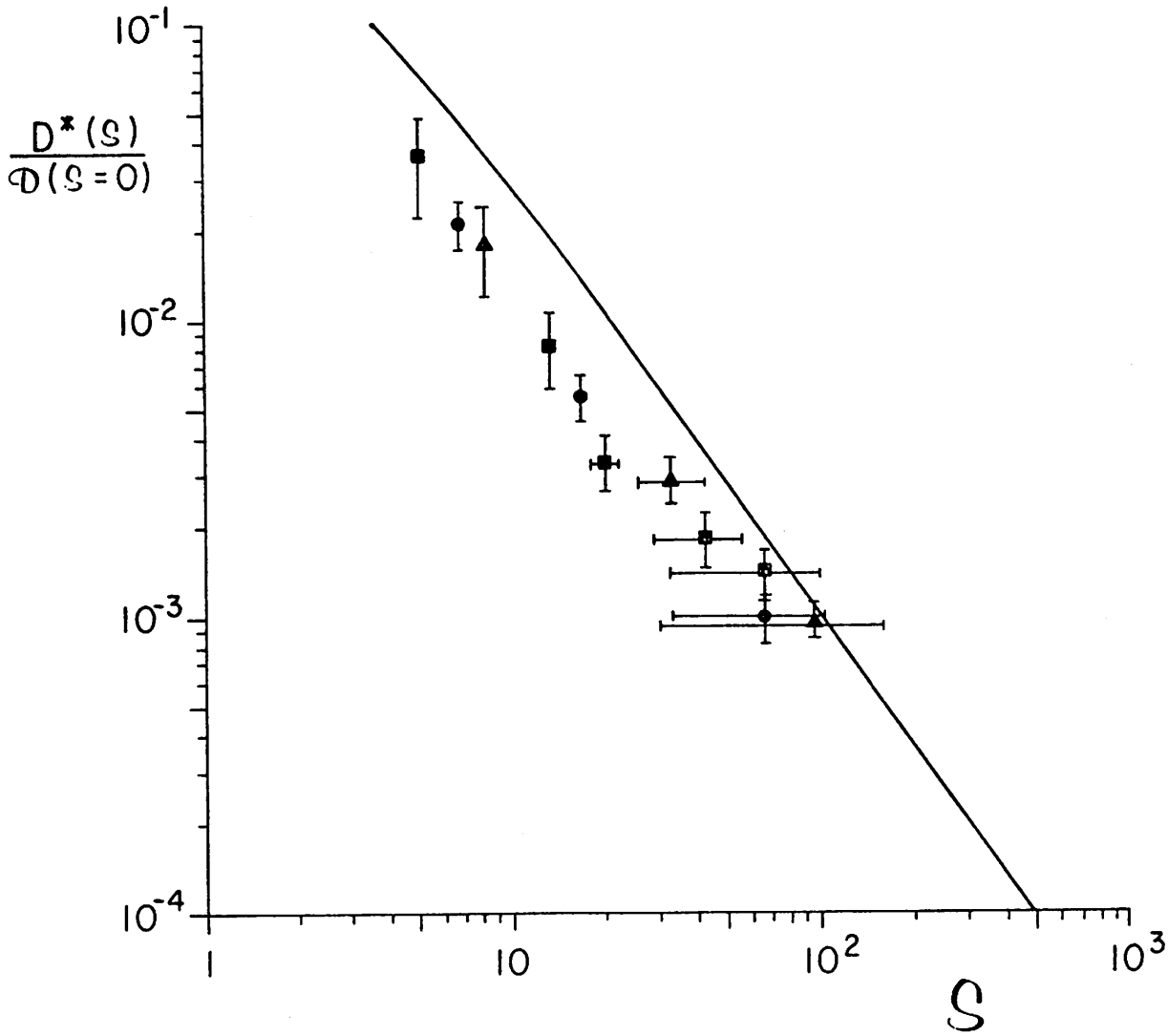

FIGURE 11. D* versus $\mathcal{S}$. $(e\Phi_o/T)$ and $v_{\phi o}/v_{te}$ were held constant at .001 and 1.414, respectively, while $(\nu_{eff}/\omega_{BOUNCE}) \leq 3.5 \times 10^{-2}$. The squares mark runs in which $k_\parallel/k$ and $k\rho_e$ were held constant at .001 and 2.4×10^{-3} while kL_s was varied. The triangles mark runs in which $k\rho_e$ and kL_s were held constant at 2.4×10^{-3} and .01 while $k_\parallel/k$ was varied. The circles mark runs in which $k_\parallel/k$ and kL_s were held constant at .001, and .01 while $k\rho$ was varied. The horizontal bars reflect the spatial resolution of the measurements. The prediction of Eq. (5.14) is shown by the solid line.

by about a factor of 0.4. This factor presumably reflects the rather large phase velocity employed in these runs, $(v_{\phi o}/v_{te}) = 1.414$. At larger values of ς, the measured values of the diffusion coefficient are somewhat larger than one might expect. This is due to insufficient spatial resolution in our measurement of D^* at large values of ς.

The computer simulations summarized in Figs. 9 - 11 confirm the scaling of the pseudoclassical transport coefficients predicted by Eq. (5.6). This confirmation, together with the smooth transition between the regimes of strong and weak magnetic shear observed in Fig. 9 provide strong support for the extension of pseudoclassical transport theory to sheared magnetic fields given by Eqs. (5.9) - (5.10).

7. CONCLUSION

We have extended previous work (Pogutse, 1972; Brambilla and Lichtenberg, 1973; Gell, et al., 1975; Nevins, 1977a) on the enhanced transport associated with the trapping of electrons in a finite amplitude electrostatic wave (pseudoclassical transport) to include simultaneously the effects of shear in the magnetic field and finite wave frequencies. As stated previously, the magnetic shear prevents the divergence of the pseudoclassical transport coefficients at the mode rational surface.

The spatial dependence of the pseudoclassical transport coefficients may be obtained by using Eqs. (3.1) and (4.8) to rewrite Eq. (5.6) in the form

$$D_p(x) = \left[1 + (x_s / x)^3\right]^{-3/2} (x_s / x)^2 D_{pc} \tag{7.1}$$

where

$$D_{pc} = \left\{ \frac{\Omega_e}{\omega} kL_s \right\}^{2/3} \left(\frac{e\Phi_o}{T} \right)^{1/2} \rho_e^2 \nu_e \tag{7.2}$$

and x_s is given by Eq. (4.17). This spatial dependence is illustrated in Fig. 12. Eq. (7.1) is shown by the solid line, while the spatial dependence obtained by previous workers (Pogutse, 1972; Gell and Nevins, 1975; Nevins, 1977a),

$$D(x) = (x_s / x)^2 D_{pc} \tag{7.3}$$

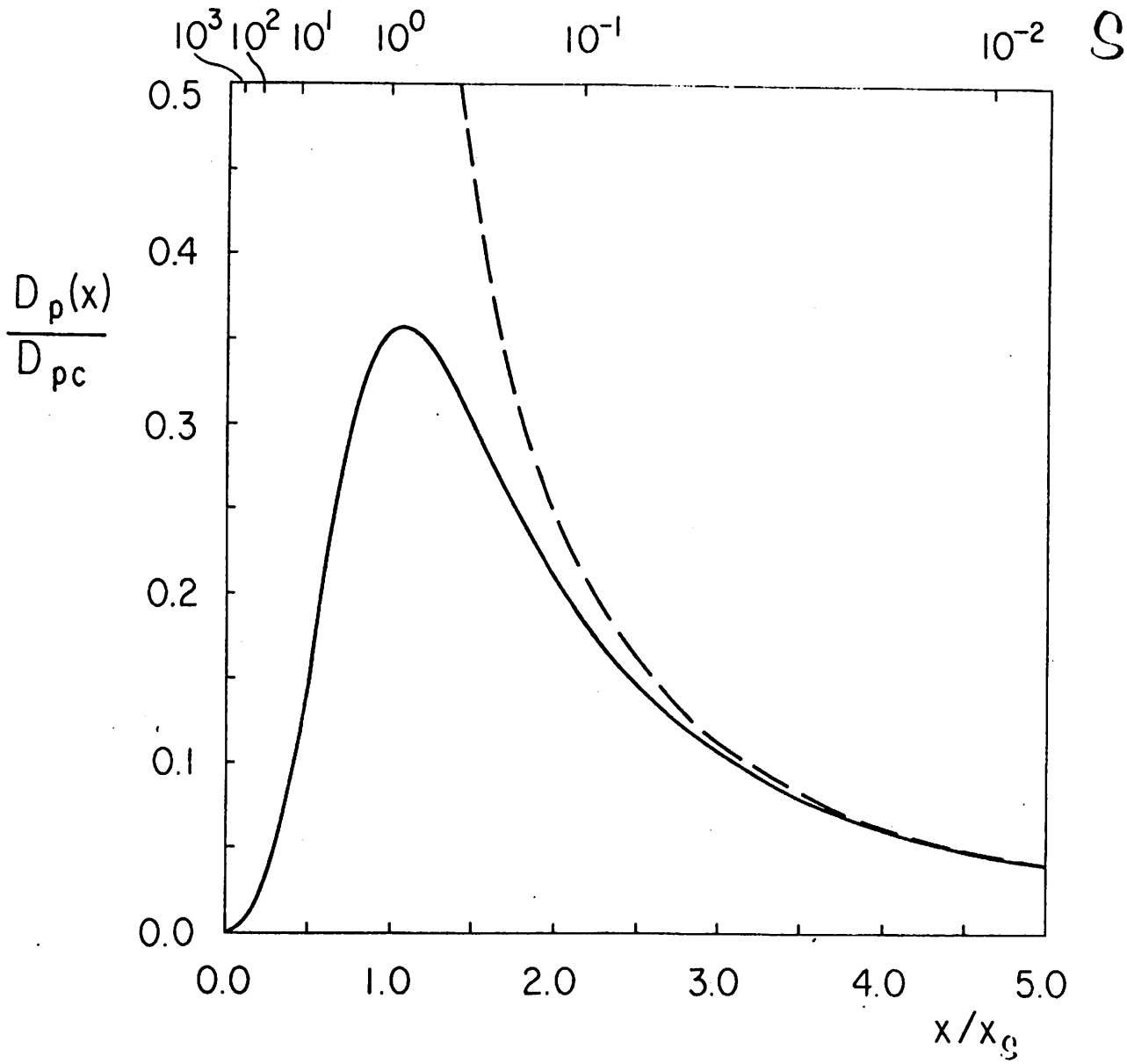

FIGURE 12. The spatial dependence of the pseudoclasical transport coefficient given by Eq. (7.1) is shown by the solid line. The spatial dependence without shear obtained by previous authors (dashed line) is included for comparison.

is shown by the dashed line. The correction to the previous work due to the shear in the magnetic field is significant for $x/x_s \lesssim 2$, and the divergence at the mode rational surface is entirely avoided.

In addition, we have tested both the kinetic calculation of the pseudoclassical diffusion coefficient of Nevins (1977a) and our extension of this result to sheared magnetic fields through the use of computer simulations. Very good agreement was found between the theory and the computer experiments.

It is evident from Fig. 12 that D_{pc} provides a characteristic value of the pseudoclassical transport coefficient that may be used to estimate a lower limit on the pseudoclassical energy confinement time, τ_E^{PC}. Normalizing the parameters to values characteristic of current tokamak experiments, we find:

$$\tau_E^{pc} \geq 2.8 \text{ msec } \frac{[T_e/1 \text{ KeV}]^{7/6} [B/10^4 \text{ gauss}]^{2/3} [L_n/10 \text{ cm}]^{4/3}}{[n/10^{14} \text{ cm}^{-3}] [(e\Phi_o/T)/10^{-2}]^{1/2} [L_s/100 \text{ cm}]^{2/3}} . \quad (7.4)$$

Since 2.8 msec is of the order of the energy confinement time observed in tokamak experiments, we conclude that the pseudoclassical transport process described here may be important in determining the energy confinement time in present and future tokamak experiments.

We present this estimate of the pseudoclassical energy confinement time only to establish the possible importance of this transport mechanism. Because of the approximate nature of the estimate, as well as the uncertainties in the dependence of the wave parameters ω, k, and $(e\Phi_o/T)$ on the parameters of the plasma, we caution against

interpreting Eq. (7.4) as a description of the scaling of the pseudoclassical energy confinement time with the plasma parameters L_n, L_S, T_e, B, and n.

Instead of merely estimating the values of ω, k, and $(e\Phi_o/T)$, a complete treatment of pseudoclassical transport must provide a means of calculating these quantities. Such a treatment of pseudoclassical transport requires knowledge of the drift wave fluctuation spectrum. The calculation of this fluctuation spectrum is the central problem in determining the anomalous transport associated with low frequency drift waves. It has been shown elsewhere (Nevins, 1977b) that the pseudoclassical particle flux can be important in determining the nonlinear evolution of this wave spectrum. Hence, the calculations of the fluctuation spectrum and the anomalous transport must be performed self-consistently.

In performing this self-consistent calculation it is important to understand the connection between the pseudoclassical transport theory considered here and other work on the anomalous transport associated with low frequency drift waves (e.g., Horton, 1976; Liu, et al., 1976; Krall and McBride, 1977). One of us has considered this problem elsewhere (Nevins, 1977b) and found that this pseudoclassical theory is a nonlinear theory of the interaction between the wave and the resonant electrons. This theory replaces the "quasilinear" treatment of this interaction at large wave amplitudes, such that inequality (5.5) is satisfied, provided that the drift wave fluctuation spectrum is sufficiently coherent.

ACKNOWLEDGMENTS

We would like to acknowledge Dr. Y. Gell for his valuable assistance in this work. In addition we are happy to acknowledge Prof. C. K. Birdsall for many helpful discussions as well as his continuing support and encouragement, Prof. A. J. Lichtenberg for many useful discussions and comments, Prof. A. N. Kaufman for naming the trapped particle orbits, and Dr. H. Okuda for suggesting the particle simulation model. Further, we would like to thank Dr. A. B. Langdon for the use of his code, ES1, that formed the basis of our diffusion code, and Drs. Lawrence Anderson and Gary R. Smith for invaluable assistance in our computational work at LBL. Finally, we thank Richard J. Meyers and Jean Yao for programming support on the MFECC computer.

This work was supported in part by the Department of Energy under Contract No. EY-76-S-03-0034-PA128.

Appendix A - THE ENERGY CONSTANT (Sect. 2)

In this appendix the energy constant E used in our interpretation of Eq. (2.15) is derived.

The energy of a particle in the "lab" frame is not conserved because the wave potential is a function of time. Hence, one must go to the "wave" frame to find an energy constant. In a uniform magnetic field this is usually accomplished by transforming to a reference frame that is moving with the velocity

$$\underline{w} = \frac{\omega}{k_{\parallel}} \hat{B} \tag{A.1}$$

relative to the lab frame. The great advantage of this choice of reference frames in a uniform magnetic field is that the induced electric field in the new frame of reference,

$$\underline{\varepsilon}_o' = \underline{w} \times \underline{B} \tag{A.2}$$

vanishes identically.

In a sheared magnetic field $\hat{B}$ becomes a function of x. Hence, $\underline{w}$ can satisfy Eq. (A.1) at only one particular value of x; and any change of reference frame in a sheared magnetic field must produce a time independent electric field, $\underline{\varepsilon}_o'$, in the new reference frame.

Finding no advantage in transforming to a reference frame moving along the magnetic field, we instead choose to transform to a frame moving parallel to the wave vactor, $\underline{k}$. Hence, choose

$$\underline{w} = \frac{\omega}{k}\,\hat{y}$$

(recall that $\underline{k} = k\hat{y}$). In this reference frame there is an electric field given by

$$\underline{\varepsilon}_o' = \frac{\omega}{k}\,B_z(x)\,\hat{x} \tag{A.4}$$

$$= -\,\nabla\Psi_o \tag{A.5}$$

where this time independent potential, Ψ_o , is given by

$$\Psi_o = -\,\frac{\omega}{k}\int^{x} B_z(x')\,dx' \,. \tag{A.6}$$

The magnetic field is unaffected by this transformation provided w is small compared to the speed of light. The phase variables of a particle transform as

$$v_\parallel' = v_\parallel - \underline{w}\cdot\hat{B}(x) \tag{A.7}$$

$$\mu' = \mu \tag{A.8}$$

$$x' = x \tag{A.9}$$

$$y' = y - wt \,. \tag{A.10}$$

In this new reference frame the wave phase,

$$\theta = k_y\,y' \,, \tag{A.11}$$

is independent of time. Hence, the total energy in this reference frame,

$$E = \tfrac{1}{2}mv_{\parallel}'^{2} + e\Phi + e\Psi_o + \mu B \qquad (A.12)$$

is conserved. Using Eqs. (A.6) thru (A.9) the energy constant may be written in terms of the phase variables in the lab frame as

$$E = \tfrac{1}{2}m\left(v_{\parallel} - \frac{\omega}{k}\frac{B_y}{B}\right)^2 + e\Phi - e\frac{\omega}{k}\int^{x} B_z(x')\,dx' + \mu B \; . \qquad (A.13)$$

Appendix B - THE DIFFUSION CODE (Sect. 6)

To verify the diffusion coefficients predicted by the theory presented here and elsewhere (Nevins, 1977a), a computer simulation code was developed. This code also proved invaluable as an independent check of our predictions of the pineapple orbit widths and of the fraction of particles trapped by the wave. The configuration of the code is exactly the same as that described in Sect. 2 (see Fig. 1). The code follows the motion of hundreds (typically 500 to 1000) of non-interacting test particles subject to externally applied electric and magnetic fields and a Monte Carlo collision operator. No self-fields are calculated. Each particle is described by the full three dimensional velocity vector. However, the particle's motion in space is projected into the x-y plane, yielding a 2D3V code. The system is periodic in the y-direction, and unbounded in the x-direction (the direction of diffusion).

The simulation code consists of three main parts. First, the particles are advanced along their cycloidal orbits, using the method of Buneman (1967), extended to allow for shear in the magnetic field (Harte and Nevins, 1976) as in Fig. 1. Because this algorithm sends the particles along their cycloidal orbits, assuming constant $\underline{E}$ and $\underline{B}$, there is no reason to choose the time step to be small in comparison to the gyro period. In fact, $\Omega\Delta t \geq 1000$ was successfully used. The time step must be choosen such that it is small compared with the time scale for changes in $\underline{E}$ and $\underline{B}$.

Second, the particles are scattered in velocity space, using the collision operator of Shanny, et al. (1967). This collision operator models the small angle, three dimensional velocity space scattering of electrons off stationary ions, and includes the $(\text{velocity})^{-3}$ dependence of the collision frequency. The statistical properties of this collision operator have been examined by Horton, et al. (1977). These authors conclude that, over many discrete time steps, this collision operator accurately models the Fokker-Planck collision operator.

Third and finally, the code calculates the mean squared displacement of the particles in x. The asymptotic value of the mean squared displacement divided by twice the time is taken to be the diffusion coefficient. Examples of this diagnostic are shown by Nevins and Harte (1976).

For each calculation the test particles are initialized with a Maxwellian velocity distribution and are loaded uniformally in the y coordinate, i.e., they are placed uniformly in the phase of the electrostatic wave. For computational simplicity, all particles are placed at $x = 0$ initially. The code then integrates the particle orbits forward in time subject to the fields and collisions; and calculates and plots $\langle \Delta x^2 \rangle / 2t$. The asymptotic value of this quantity is D^*, while the fluctuations in this quantity provide the vertical error bars shown in Figs. 5-11.

Orbit plots can also be generated by this code. Figs. 2 and 3 show some of these orbits. In generating these orbits the collision frequency was set to zero.

Appendix C - THE INFLUENCE OF THE POLARIZATION DRIFT ON THE TRAPPED PARTICLE ORBITS (Sect. 2)

It has been suggested on several occasions that we should consider the effect of the polarization drift on pseudoclassical transport in the "pineapple" regime. In this regime pseudoclassical transport results from the trapping of electrons by the finite amplitude electrostatic wave. Hence, we consider the influence of the polarization drift on the orbits of electrostatically trapped electrons.

The polarization drift velocity, $\underline{V}_p$, is given by

$$\underline{V}_p = \frac{1}{\Omega_e} \frac{\dot{\underline{E}}_\perp}{B} \tag{C.1}$$

where $\dot{\underline{E}}_\perp$ is the time derivative of the component of the electric field perpendicular to $\underline{B}$, taken along the particle orbit. For trapped particles we may estimate $\dot{\underline{E}}_\perp$ as

$$\dot{\underline{E}}_\perp \simeq \omega_{BOUNCE}\, \underline{E}_\perp \quad . \tag{C.2}$$

Hence, the ratio of the polarization drift velocity to the $E \times B$ drift velocity is given in order of magnitude by

$$\frac{|V_p|}{|V_E|} \simeq 7.5\times10^{-5} \frac{[k_\parallel/.1\ \mathrm{cm}^{-1}]\,[(e\Phi_o/T)/10^{-2}]^{\frac{1}{2}}\,[T_e/1\ \mathrm{KeV}]^{\frac{1}{2}}}{[B/10^4\ \mathrm{gauss}]} \quad . \tag{C.4}$$

Although the polarization drift is insignificant in comparison to the $E \times B$ drift, it still may be important in determining the period

of the trapped particle orbits because $\underline{V}_p$ has a component parallel to $\underline{k}$. Hence, the polarization drift gives an additional term in the equation for the evolution of the wave phase, θ [i.e., Eq. (5.2)]. The importance of this term may be estimated by considering $\Delta\theta_p$, the change in wave phase over one bounce period due to this term. We find

$$\frac{\Delta\theta_p}{2\pi} \simeq \frac{kV_p}{\omega_{BOUNCE}}$$

$$\simeq k^2\rho_e^2 \, (e\Phi_o/T) \; . \qquad (C.5)$$

Low frequency drift waves generally attain their largest growth rates when $k\rho_i \sim 1$. Hence, the right hand side of Eq. (C.5) may be estimated by

$$\frac{\Delta\theta_p}{2\pi} \simeq \frac{m_e}{m_i} \, (e\Phi_o/T)$$

$$\simeq 5\times10^{-6} \, [m_i/m_p]^{-1} \, [(e\Phi_o/T)/10^{-2}] \qquad (C.6)$$

where m_p is the mass of a proton. We feel quite justified in neglecting this term.

REFERENCES

1958 Rosenbluth, M. N. and Kaufman, A. N. "Plasma Diffusion in a Magnetic Field." Phys. Rev. 109, pp. 1-5, January.

1963 Galeev, A. A., Oraevskii, V. N. and Sagdeev, R. Z. "'Universal' Instability of an Inhomogeneous Plasma in a Magnetic Field," Sov. Phys. JETP 17, pp. 615-620, September 1963. [Russian original in Journal Exptl. Theoretical Physics (USSR) 44, pp. 903-911, March 1963]

1965 Braginskii, S. I. "Transport Processes in a Plasma", Rev. Plasma Phys. 1, (New York: Consultants), pp. 205-311.

Kadomtsev, B. B. Plasma Turbulence (New York: Academic Press).

1967 Buneman, O. "Time Reversible Difference Procedures," J. Computational Physics 1, pp. 517-535, June.

Shanny, Ramy, Dawson, John M. and Greene, John M. "One Dimensional Model of a Lorentz Plasma," Phys. Fluids 10, pp. 1281-1287, June.

Stix, T. H. "Resonant Diffusion of Plasma across a Magnetic Field," Phys. Fluids 10, pp. 1601-1614, August.

1968 Galeev, A. A. and Sagdeev, R. Z. "Transport Phenomena in a Collisionless Plasma in a Toiroidal Magnetic System," Sov. Phys. JETP 26, pp. 233-240, January. [Russ. Orig. in Eksp. Teor. Riz. 53, pp. 348-359, July 1967]

1969 Kadomtsev, B. B. and Pogutse, O. P. "Dissipative, Trapped-Particle Instability in a Dense Plasma," Sov. Phys. Doklady 14, pp. 470-472, November. [Russian original in Doklady Akademii Nauk SSR 186, pp. 553-556, May 1969.]

Sagdeev, R. Z. and Galeev, A. A. Non-Linear Plasma Theory, (New York: W. A. Benjamin).

1970 Stringer, T. E. "Equilibrium Diffusion Rate in a Toroidal Plasma at Intermediate Collision Frequencies", Phys. Fluids 13, pp. 810-819 (March, 1970).

1971 Politzer, P. A. "Drift Instability in Collisionless Alkali Metal Plasmas", Phys. Fluids 14, pp. 2410-2425 (November).

Yoshikawa, S. and Christofilos, N. C. "Implications of Pseudoclassical Diffusion for Toroidal Confinement Devices." In Plasma Physics and Controlled Nuclear Fusion Research (Proceedings of the Madison Conference, June 17-23, 1971), IAEA Vienna, 1971, Vol. II, pp. 357-372, and references cited therein.

1972 Pogutse, O. P. "A Possible Mechanism for Energy Losses in a Tokamak Device", Nuclear Fusion 12, 39-43, January.

Rosenbluth, M. N. Hazeltine, R. D. and Hinton, F. L. "Plasma Transport in Toroidal Confinement Systems," Phys. Fluids 15, pp. 116-140, January.

1973 Brambilla, M. and Lichtenberg, A. J. "Drift-Surface-Island Formation and Particle Diffusion in a Toroidal Plasma", Nuclear Fusion 13, pp. 517-520 (August).

1974 Dean, S. O., Callen, J. D., Furth, H. P., Clarke, J. F., Ohkawa, T., and Rutherford, P. H. Status and Objectives of Tokamak Systems for Fusion Reserach, U.S. Govt. Printing Office, Washington, D.C.

Gell, Y., Harte, J., Lichtenberg, A. J. and Nevins, W. M. "Charged Particle Orbits in Sheared Magnetic Field; Implications to Diffusion," PRL 35, pp. 1642-1645, December.

Mikhailovskii, A. B. Theory of Plasma Instabilities 2 (New York: Consultants' Bureau).

Prager, S. C. Sen, A. K. and Marshall, T. C. "Dissipative Trapped-Electron Instability in Cylindrical Geometry," PRL 33, pp. 682-695, September.

1975 Gell, Y., Harte, Judith, Lichtenberg, A. J. and Nevins, W. "Charged Particle Orbits in Sheared Magnetic Field; Implications to Diffusion," PRL 35, pp. 1642-1645, December.

Gell, Y. and Nevins, W. M. "A Variational Approach to Pseudo-classical Diffusion", Nuclear Fusion 15, pp. 1083-1089, December.

1976 Harte, J. and Nevins, W. M. "Diffusion Codes" (Electronics Research Laboratory, University of California, Berkeley: Second Quarter Progress Report on Plasma Computational Physics, July).

Harte, Judith and Nevins, W. M. "Diffusion Codes" (Electronics Research Laboratory, University of California, Berkeley: Third Quarter Progress Report on Plasma Computational Research, October).

Hinton, F. L. and Hazeltine, R. D. "Theory of Plasma Transport in a Toroidal Confinement System", Rev. Mod. Phys. 48, pp. 239-307, April.

Horton, Wendell. "Drift Wave Stability of Inverted Gradient Profiles in Tokamaks", Phys. Fluids 19, pp. 711-718, May.

Liu, C. S., Rosenbluth, M. N. and Tang, W. M. "Dissipative Universal Instability due to Trapped Electrons in Toroidal Systems and Anomalous Diffusion", Phys. Fluids 19, pp. 1040-1044, July.

Mazzucato, E. "Small-Scale Density Fluctuations in the Adiabatic Toroidal Compressor", PRL 36, pp. 792-794, April.

Nevins, W. M. and Harte, Judith. "Diffusion Model Using an External Wave and a Model Collision Operator", (Electronics Research Laboratory, University of California, Berkeley: First Quarter Progress Report on Plasma Computational Research, April), pp. 9-47.

Surko, C. M. and Slusher, R. E. "Study of the Density Fluctuations in the Adiabatic Toroidal Compressor Tokamak Using CO_2 Laser Scattering", PRL 37, pp. 1747-1750, December.

1977 Horton, Wendell, Jr., Estes, R. and Choi, Duk-In, "Properties of the Monte-Carlo Lorentz Collision Operator", Phys Fluids 20, pp. 1089-1093, July.

Koch, R. A. and Tang, W. M. "Doppler Shift Interpretation of Drift-Wave Frequency Spectrum", Bull. Am Phys. Soc. 22, p. 1143, October.

Krall, N. A. and McBride, J. B. "Quasilinear Model for Heat Flow and Diffusion in a Micro-Unstable Tokamak", Nuclear Fusion 17 pp. 713-720, August.

Manheimer, W. M. "An Introduction to Trapped-Particle Instability in Tokamaks", National Technical Information Service, Springfield, Virginia.

Miner, W. H. and Ross, D. W. "A Numerical Investigation of the Two-Dimensional Structure of the Trapped Electron Mode in Tokamaks", Bull. Am. Phys. Soc. 22, p. 1167, October.

(a) Nevins, W. M. "Pseudoclassical Transport I: The Particle and Energy Flux", submitted for publication.

(b) Nevins, W. M. "Pseudoclassical Transport II: A Nonlinear Theory of the 'Collisionless' Drift Instability", submitted for publication.

(c) Nevins, W. M. "A Thermodynamic Approach to Dissipative Drift Instabilities", submitted for publication.

_____ "A Physical Interpretation of Dissipative Drift Instabilities." Presented at Annual Controlled Fusion Theory Conference, May 4-6 1977, San Diego, California.

Okabayashi, M. and Arunasalem, V. "Study of Drift-Wave Turbulence by Microwave Scattering", Nuclear Fusion 17, pp. 497-513, June.

Rewoldt, G. Tang, W. M. Frieman, E. A. "Two-Dimensional Spatial Structure of Drift, Trapped-Electron, and Shear-Alfvén Modes", Bull. Am. Phys. Soc. 22, p. 1142, October.

Ross, D. W. Hazeltine, R. D. Hinton, F. L. Strauss, H. R. "Unified Theory of Drift Waves and Tearing Modes", Bull. Am. Phys. Soc. 22, p. 1142, October.

Smith, Julius, Whitson, J. C. "A Numerical Study of the System of Differential Equations for the Drift Wave in Tokamaks", Bull. Am. Phys. Soc. 22, p. 1165, October.

Vojtsenya, V. S. Yoloshko, A. Yu, Zalkind, V. M., Solodovchenko, S. I., Tarasenko, V. P., Stan', A. F. "The Effect of Shear on Turbulent Diffusion in a Microwave Discharge Plasma in a Toroidal Stellerator", Nuclear Fusion 17, pp. 651-658, August.